This is a repository copy of *A late Wisconsin (32–10k cal a BP) history of pluvials, droughts and vegetation in the Pacific south-west United States (Lake Elsinore, CA)*.

White Rose Research Online URL for this paper:
http://eprints.whiterose.ac.uk/127832/

Version: Accepted Version

Article:

Kirby, M.E., Heusser, L., Scholz, C. et al. (9 more authors) (2018) A late Wisconsin (32–10k cal a BP) history of pluvials, droughts and vegetation in the Pacific south-west United States (Lake Elsinore, CA). Journal of Quaternary Science, 33 (2). pp. 238-254. ISSN 0267-8179

https://doi.org/10.1002/jqs.3018

Reuse
Items deposited in White Rose Research Online are protected by copyright, with all rights reserved unless indicated otherwise. They may be downloaded and/or printed for private study, or other acts as permitted by national copyright laws. The publisher or other rights holders may allow further reproduction and re-use of the full text version. This is indicated by the licence information on the White Rose Research Online record for the item.

Takedown
If you consider content in White Rose Research Online to be in breach of UK law, please notify us by emailing eprints@whiterose.ac.uk including the URL of the record and the reason for the withdrawal request.

eprints@whiterose.ac.uk
https://eprints.whiterose.ac.uk/

A late Wisconsin (32-10k cal a BP) history of pluvials, droughts, and vegetation in the Pacific southwest United States (Lake Elsinore, CA).

*Kirby, M.E.[a], Heusser, L.[b], Scholz, C.[c], Ramezan, R.[d], Anderson, M.A.[e], Markle B.[f], Rhodes, E.[g], Glover, K.A.[h], Fantozzi, J.[a], Hiner, C.[a], Price, B.[a], Rangel, H.[a]

[a] *Department of Geological Sciences, California State University, Fullerton, Fullerton, CA 92834 USA* (mkirby@fullerton.edu); [b] *Lamont-Doherty Earth Observatory of Columbia University, Palisades, NY 10601 (heusser@ldeo.columbia.edu), USA*; [c] *Department of Earth Sciences, Syracuse University, Syracuse, NY USA 13244* (cascholz@syr.edu); [d] Department of Mathematics, California State University, Fullerton, Fullerton, CA 92834, [e] University of California Riverside, Department of Environmental Sciences, Riverside, CA 92521; [f] *Quaternary Research Center and Department of Earth and Space Sciences, University of Washington, Seattle, Washington 98195, USA* (bradley.markle@gmail.com); [g] *Geography, University of Sheffield, Sheffield, United Kingdom* (ed.rhodes@sheffield.ac.uk); [h] Climate Change Institute, University of Maine, Orono, ME 04469 (katherine.glover@maine.edu).

*corresponding author

Running Head: California's glacial history of pluvials, droughts, and vegetation

Keywords: Lakes, sediment, Glacial, California, drought, insolation

ABSTRACT: Continuous, sub-centennially resolved, paleo terrestrial records are rare from arid environments such as the Pacific southwest United States. Here, we present a multi-decadal-to-centennial resolution sediment core (Lake Elsinore, CA) to reconstruct late Wisconsin pluvials, droughts, and vegetation. In general, the late Wisconsin is characterized by a wetter and colder climate than during the Holocene. Specifically, conditions between 32.3-24.9k cal a BP are characterized by large amplitude hydrologic and ecologic variability. Highlighting this period is ~2000-year glacial mega-drought (27.6-25.7k cal a BP) during which the lake shallowed (3.2-4.5 m depth). This period is approximately coeval to a Lake Manix regression and an increase in xeric vegetation in the San Bernardino Mountains (Baldwin Lake). The Local Last Glacial Maximum (LLGM) is bracketed between 23.3-19.7k ca a BP – a ~3000-year interval characterized by reduced run-off (relative to the glacial), colder conditions, and vegetative stability. Maximum sustained wetness follows the LLGM, beginning at 19.7 and peaking by 14.4k cal a BP. A two-step decrease in runoff characterizes the late glacial to Holocene transition; however, the vegetation change is more complex, particularly at the beginning of the Younger Dryas chronozone. By 12.6-12.4k cal a BP, the climate achieved near Holocene conditions.

Introduction and Background

The Pacific southwest United States (pswUS) is a perennially water-stressed and over-populated region. This stress is unlikely to diminish in the future as droughts become more frequent and severe (Neelin et al., 2013; Seager et al., 2013; Kam and Sheffield, 2016). At the same time, the intensity of precipitation could increase as well, exacerbating risk associated with floods and their related hazards (Berg and Hall, 2015; Yoon et al., 2015; Shields and Kiehl, 2016). Preparing for these scenarios and mitigating their impact is key to maintaining the region's population and its socioeconomic vitality. Key to preparation and mitigation is a paleo perspective. Paleo perspectives inform on the range of climatic possibilities such as drought and floods. Included in this paleo perspective is the role that changes in climate play on vegetative structure. In the pswUS, native vegetation is highly stressed resulting in its inclusion as one of the world's 25 biodiversity hotspots (Myers et al., 2000). Known as the California Floristic Biodiversity Hot Spot, this region is experiencing, and will continue to experience, threats associated with climate change. In this paper, we use sediments from Lake Elsinore, California to gain paleo perspectives on hydroclimates and their relationship to vegetation between 32 and 10k cal a BP. Specifically, we build on, and add to, existing vegetative (32.6-9k cal a BP, Heusser et al., 2015) and the deglacial (19-9k cal a BP, Kirby et al., 2013) reconstructions by updating the age model, adding indicators of runoff from 32-17k cal a BP, and examining the relationship between the runoff and vegetation between 32-10k cal a BP. We focus specifically on a prolonged dry interval between 27.6-25.7k cal a BP, with consideration for regional comparisons. We begin this paper with a brief review of Kirby et al. (2013) and Heusser et al. (2015).

Kirby et al. (2013) document the late glacial to Holocene transition (19-9k cal a BP) using a combination of sediment grain size to infer runoff and C_{28} *n*-alkanoic acids from plant leaf waxes (∂D_{wax}) to infer moisture source. In general, runoff decreases from 19-9k cal a BP with notable shifts to less runoff at the start of the Bolling-Allerod (B-A) (14.7k cal a BP) and then again at the start of the Younger Dryas (YD) (12.9k cal a BP). A comparison to known forcings such as the Atlantic Meridional Overturning Circulation (AMOC), ice sheet area, and CO_2 radiative forcing reveal potential causative relationships. Notably, the long term decrease in wetness from 19-9k cal a BP mirror both loss of ice sheet volume and an increase in CO_2 radiative forcing. Together, these changes may have gradually shifted the mean winter storm track north from 19-9k cal a BP. Alternatively, the storm track may have experienced very little latitudinal changes, instead reflecting a change in the frequency and/or intensity of southward tracking storms as climate transitioned from a glacial state to a Holocene state (Antevs, 1948; Wells et al., 2003; Kirby et al., 2013; Ibarra et al., 2014; Löfverström et al., 2014; Oster et al., 2015; Wong et al., 2016; Lora et al., 2016). The ∂D_{wax} mirror this gradual decrease in wetness suggesting a change in dominant moisture sources from higher latitude sourced (or colder storms) to lower latitude sourced (or warmer storms) winter storms between 19-9k cal a BP. The ∂D_{wax} do not indicate a tropical or subtropical moisture source during the late glacial as proposed by Lyle et al. (2012). Superimposed on this gradual drying trend are shifts in wetness at 14.7 and 12.9k cal a BP. These shifts are proposed to be coeval to shifts in AMOC strength. Consequently, the pswUS late glacial to Holocene transition is likely forced by a combination of external drivers associated with ice sheet dynamics and radiative forcing as well as oceanic forcing associated with conditions in the North Atlantic.

Heusser et al. (2015) examine the pollen data between 32.6-9k cal a BP. Results show a generally more mesic vegetation than today during the last glacial. Evidence for shifts in vegetation, particularly between 27.5-25.5k cal a BP (27.6-25.7k cal a BP as per updated age model – this paper), suggest a significant vegetative response. The latter 2000-year interval is interpreted as a return to more xeric vegetation reflecting a more arid climate. A comparison to pollen from Santa Barbara Basin show generally similar millennial scale features as Lake Elsinore (Heusser, 1995; Heusser and Sirocko, 1997). However, as Heusser et al. (2015) notes, the 2000-yr glacial mega-drought is missing from the Santa Barbara Basin pollen record, suggesting that the terrestrial Lake Elsinore pollen site may capture changes absent in its marine counterpart (Heusser, 1995; Heusser and Sirocko, 1997).

Study Site

Modern climate setting

The climate of the pswUS is Mediterranean, characterized by wet, cool winters and hot, dry summers. In general, the coastal plain and low-lying inland regions receive less precipitation than the adjacent mountain ranges (Masi, 2005). In particular, tropical (El Niño Southern Oscillation (ENSO)) and extratropical (Pacific Decadal Oscillation (PDO)) Pacific Ocean-atmosphere conditions influence the climate of the pswUS (Cayan and Peterson, 1989; Cayan et al., 1999; Brito-Castillo et al., 2003; Hanson et al., 2006). Pacific Ocean-atmosphere conditions modulate the mean winter position of the eastern Pacific subtropical high (Cayan and Peterson, 1989; Hanson et al., 2006). When the jet stream is south it results in higher than average precipitation and associated river discharge, while a more northerly position of the jet steam results in lower than average precipitation and less river discharge (Cayan et al., 1999; Hanson et al., 2006). Most importantly for our paleo studies is that the pswUS is a relatively simple, unimodal precipitation regime as compared to its interior southwest US counterparts (Kirby et al., 2013). Consequently, the hydroclimatic paleo interpretation is straightforward – indicators of wet climates are caused by wetter winters and vice versa for dry climate indicators. Finally, it is well documented that changes in precipitation in the pswUS are positively correlated to both changes in regional lake level and changes in the flux, and size, of sediment in regional rivers, illustrating the modern link between climate and sedimentation in the study region (Inman and Jenkins, 1999; Warrick et al., 2004, 2007, 2015; Romans et al., 2009; Covault et al., 2010; Xu et al., 2010; Kirby et al., 2010, 2013, 2014; Gray et al., 2014, 2015; Hiner et al., 2016).

Tectonic setting

Lake Elsinore is a pull-apart basin along the Elsinore Fault zone formed by fault step-over movement along the strike-slip Wildomar Fault to the Glen Ivy North Fault (Mann, 1956; Hull, 1990) (Figure 1). Gravimetric studies reveal an approximately 1000 m thick sediment package within the basin (Hull, 1990). The basement rocks are granitic and date to the late Cretaceous (Krummenacher et al., 1975; Silver et al., 1979).

At Lake Elsinore fault dip is near vertical and seismic activity is low (Krummenacher et al., 1975). Only two moderate earthquakes have been recorded in the northern Elsinore fault zone over the past 200 years ($M \leq 6$, Toppozada et al., 1978). Along the southern section of the Elsinore fault zone, approximately 40 km to the SE of Lake Elsinore, a minimum of four earthquakes ($M \leq 4.5$) have generated surface rupture over the last 4,500 years (Vaughan et al., 1999). Available data on fault slip rates suggest that the horizontal to vertical slip ratio is in excess of 10:1 (Hull and Nicholson, 1992). Horizontal separation is estimated at 10 to 15 km over the past ~2.5 Ma based on offset features observed in bedrock, most notably changes in foliation dip; only minimal vertical offset has been identified (Weber, 1977; Morton and Miller, 1987).

From this tectonic interpretation, it is concluded that hydrologically-produced, vertical changes in the lake's base level greatly exceed earthquake-generated vertical changes. Under modern conditions, these hydrologically-produced changes can exceed 13 m (Kirby et al., 2004). In other words, complete desiccation of modern Lake Elsinore results from a 13 m drop in base-level (Kirby et al., 2004). Vertical changes due to fault rupture are small (< 1-2 m) based on paleo seismic data (Vaughan et al., 1999). This extreme disparity between hydrologic and tectonic forced base level change suggests that vertical motion related to tectonics is not the primary determiner of the lake's changing sedimentation and stratal geometries, especially over the geologically short periods of time analyzed in this paper. Of course, on longer timescales, the basin's rate of fault-related vertical subsidence must exceed average sedimentation rates in order for the basin to exist as depositional feature. As a test of this statement, we collected seismic reflection data to examine the basin's long-term sedimentation and stratal geometries, with the purpose to identify potential basin faulting and its influence on sedimentation (see Discussion).

Limnology

Lake Elsinore is a shallow, polymictic lake (Anderson, 2001). The hypolimnion experiences short periods of anoxia, but wind mixing of epilimnic oxygen rich waters into the hypolimnion inhibits prolonged anoxia, under modern conditions (Anderson, 2001). The occurrence of laminae during parts of the glacial suggest a deeper lake (perhaps anoxic) at times (Kirby et al., 2013). The lake's water budget is controlled by a combination of outputs such as evaporation, (>1.4 m yr^{-1}, Anderson, 2001) and occasional overflow. Inputs include direct runoff from its main influent, the San Jacinto River, as well as runoff from the adjacent Elsinore Mountains. The role ground water plays in the lake's hydrologic budget is less well known (Damiata and Lee, 1986; Thiros, 2010). The main outlet is located along the north side of the lake. Twenty brief overflow events into northwest flowing Walker Canyon have occurred since 1769 AD, including three times in the 20th century (Lynch, 1931). Consequently, the lake is sometimes a terminal basin (closed) and at other times a through-flow basin (open). Modern maximum lake level depth is ~13 m before overflow occurs, based on the modern sill elevation (Anderson, 2001). It is unknown how the spill elevation has changed through geologic time. Historically the lake has desiccated on several occasions since 1769 AD, most recently in the 1950's (Lynch, 1931). During the 1950's drying episode, the lake's central basin remained a wet, muddy environment (Hudson, 1978). The 1950's drying event is recognized in sediment cores as a low water content, stiff crumbly clayey-silt unit with low sand content (Kirby et al., 2004, 2010).

Methods

Age control

Twenty-eight AMS radiocarbon ages on discrete organics (e.g., wood, charcoal), bulk $C_{org.}$, gastropod shells, or paired discrete-bulk $C_{org.}$ materials were measured at the University of

California, Irvine W. M. Keck Carbon Cycle Accelerator Mass Spectrometry Laboratory or the Lawrence Livermore National Laboratory (Table 1). Discrete and bulk $C_{org.}$ samples were prepped using a standard acid-base-acid pretreatment. The gastropod shells were leached of 50% of their mass using HCl to remove secondary carbonate. Two Infra-Red Stimulated Luminescence (IRSL) dates from single grains (175–200 µm) of K-feldspar were obtained from two silty-sand units (2438 – 2452 cm and 2500 – 2517 cm) at the University of California, Los Angeles following standard lab protocol (Rhodes, 2015). An age model was created using 28 radiocarbon ages entered into the Bacon (v.2.2, IntCal13) age-modelling software (Blaauw and Christen 2011) (Table 1). The IRSL ages are not included in the age model calculation.

Sediment and pollen analyses

Core LEDC10-1 was extracted from 7 m water depth over three days in June 2010 using a hollow stemmed auger push core system with a lined hole aboard a stabilized coring barge (Figure 1). Each drive was 0.61 m and recovery was better than 90% for the total core length. Core acquisition started at 9 m below the sediment-water interface and ended at 30 m. The cores were capped, labeled and transported back to the Cal State Fullerton Lab where they we opened, described, and digitally photographed. 4-5 grams of wet sediment was extracted at 1 cm contiguous intervals for magnetic susceptibility measurements, percent total organic matter (LOI 550 °C), and percent total carbonate (LOI 950 °C). Samples for grain size analysis were extracted every other cm for determination using a Malvern laser diffraction grain size analyzer. Each grain size sample was pretreated using 30 mL 30% H_2O_2 to remove organic matter, 10 mL 1N HCl for carbonate removal, and 10 mL 1N NaOH for biogenic silica removal. Complete measurement details for all sediment analyses are provided in Kirby et al. (2013). The same set of grain size methods were determined for the surface sediment samples collected by Anderson (2001). Pollen methods, results, and statistical analyses are described in Heusser et al. (2015).

To determine statistically significant break-points in the percent total sand data, we use a sequential regime shift detection program (SRSD v.6.2 https://sites.google.com/site/climatelogic/) by Rodionov (2004, 2015) – the same as that used by Kirby et al. (2014) for Zaca Lake. The data were separately analyzed pre- and post- 27.6-25.7k cal a BP to avoid the exceptionally high sand content unit. Targeted significance level was $p < 0.05$ with a cut-off data point length of 20 and a Huber's tuning constant of 2. Red noise estimation was not included (Rodionov, 2004, 2015). The purpose of this analysis is to provide a statistical (non-subjective) basis for subdividing the sand data into statistically significant intervals. This method removes the subjectivity often associated with visually assigned break points in otherwise complex, variable time series data. Because the grain size data were sampled at a higher resolution than the pollen data, we use the SRSD intervals (rather than the pollen zones from Heusser et al., 2015) as the focus of our discussion section.

Modern lake bottom surface sand values were plotted versus modern water depth (ca. 2001 AD) and analyzed using nonlinear regression with bootstrap confidence intervals. Following least squares approach, the parametric curve $Depth = b_0 + b_1(percent\ total\ sand)^{b_2}$ was fitted to the data. The quantiles of 1,000 bootstrap samples were used to estimate the uncertainty around the fitted model. Grain size distributions were also plotted for a modern Lake Elsinore beach sample and for all modern lake bottom sediment samples between 6.01 and 7.32 m water depth. The same plots were made for SRSD intervals 1-7 and 9-14 as well as SRSD 8 – the glacial sand unit.

Seismic reflection data

Twenty high-resolution single-channel seismic reflection profiles, totaling ~ 75 km in length, were used to investigate Lake Elsinore's sub bottom (Figure 1). Seismic reflection profiles were collected using both a shallow, high-resolution system (4-24 kHz CHIRP) and a deeper-penetrating, lower-frequency source system (1 kHz Boomer), with position information provided by a differential GPS navigation system. The 1kHz seismic data were recorded digitally at a sampling interval of 0.125 ms. A velocity of 1500 m/sec was used for data processing (Scholz, 2001). Raw seismic data files were transferred into ProMax seismic processing software. Raw data were processed using four separate filters (Yilmaz, 2001). A spiking/ predictive deconvolution and a bandpass filter were used to attenuate ringing of the shallow water data sets and eliminate extraneous coherent noise. A trace-mixing filter was applied to the seismic data to further diminish random noise and enhance signals from the sedimentary record. In addition, an automatic gain control function, which counteract the natural attenuation of the seismic signal with depth, was used to enhance the later (deeper) seismic arrivals. Processed lines were transferred to Seisworks-2D for final seismic reflection analysis and interpretation.

Results

Age control

The twenty-eight, radiocarbon based age model is updated from Kirby et al. (2013) and Heusser et al. (2015) (Figure 2, Table 1). Figure 2b and 2c show the differences between the former age model used by Kirby et al. (2013) and Heusser et al. (2015) and that determined for this paper. Importantly, this updated age model does not invalidate interpretations in Kirby et al. (2013) or Heusser et al. (2015). For example, the absolute ages of the pollens zones determined in the Heusser et al. (2015) paper move up-time or down-time respectively; however, the statistical basis for these pollen zones is time independent. Three bulk organic carbon dates used in Kirby et al. (2013) and Heusser et al. (2015) are not used in this paper's age model (1747-1748 cm, 1823-1824 cm, and 2019-2020 cm). Eight new age control points are added to this paper including: 1723-1725 cm, 2280-2282 cm, 2292-2293 cm, 2384-2386 cm, 2425-2427 cm, 2830-2832 cm, and 2 x 2860-2861 cm (Table 1). Overall, the age model indicates relatively linear sedimentation between 32-10k cal a BP (0.08 cm^{-1} year or 13.1 years cm^{-1}).

Sedimentology

Core LEDC10-1 consists predominantly of clayey silts with minor sand contributions (< 20 %) (Figure 3 and S1). The average time step between individual grain size analyses is 30 years (Figure S2). Organic matter and carbonate make up less than < 20 % of the total sediment material, in general. The sediment is variably laminated in places and occasionally massive (Figure 3). A notable increase in organic matter occurs between ~25-23k cal a BP and to a lesser extent between 31-30k cal a BP. Carbonate is virtually absent between 32-14k cal a BP; however, it increases dramatically at ~14k cal a BP and into the Holocene (Kirby et al., 2007, 2013). A distinct sand-dominated unit occurs between 27.6-25.7k cal a BP (Figure 3 and S1). SRSD analysis defines thirteen statistically significant ($p < 0.05$) break points in the sand data. We assign the glacial sand layer its own interval, thus bringing the total defined sand intervals to fourteen (Figure 4). All of SRSD sand intervals, except the youngest (1) and the oldest (14), average percent total sand values higher than the Holocene average (Figure 4). Modern lake bottom sediment samples reveal a decrease in total sand with increasing water depth (Figure 5). Grain size plot distributions show that silty clay dominates the modern lake bottom samples between 6.01 and 7.32 m water depth as well as the SRSD intervals 1-7 and 9-14 (Figure 6). Conversely, the modern beach sample and glacial sand unit (SRSD 8) are coarser, characterized by sand and sandy silt, respectively. Pollen results are discussed in detail by Heusser et al. (2015). The average time step between individual pollen analyses is 92 years with intervals of higher resolution data across zones of interest (Figure S2).

Seismic reflection data

Two representative seismic reflection lines acquired using the 1 kHz Boomer system are shown on Figure 7. LE line 10 was collected along the lake's long axis while LE line 33 was collected along the short axis. The two lines intersect very near the core location used for this study (Figure 1, LEDC10-1). Image quality diminishes with depth, likely the result of gas-produced signal attenuation. Nonetheless, faint sub-parallel reflectors are observed to about 60-70 m below the lake bottom. In general, the two lines show moderate divergent basin fill stratal geometries with parallel to sub-parallel reflectors (Figure 7).

Discussion

Basin analysis

The seismic reflection data reveal a basin fill geometry typically associated with pull-apart basins such as moderate divergent fill geometries characteristic of sediment focusing (Figure 7) (Blais and Kalff, 1995; Csato et al., 1997; Enzel et al., 2006). Reflectors are strongest in the upper 10 m of the sediment package, corresponding to the Holocene. Within the upper 10 m, there is some evidence for laterally discontinuous reflectors, possibly truncation and offlapping, suggesting periods of lake surface area contraction (i.e., low lake level) (Kirby et al., 2004; Pyke, 2013). Reflectors deeper than 10 m (glacial-age), are less prominent, exhibit less divergence, and are more laterally continuous in terms of stratal thickness. This change from the Holocene to the glacial likely reflects the generally wetter glacial climate and the subsequently larger lake surface area associated with greater runoff (see discussion below). As a result, the area of sedimentation expanded within the glacial basin creating a more uniformly thick sediment package with little expression of tapering shoreward. At the time of data acquisition, the lake's surface elevation was unusually low; consequently, we were unable to collect data at the far edges of the basin where lateral displacement associated with the Wildomar or Glen Ivy faults is anticipated (Figure 1). Importantly, there is no evidence of central-basin faulting, large-scale erosional truncation, or prograding clinoforms (deltaic migration). The absence of these features suggests that the sediment core contains a relatively continuous sediment history.

A late Wisconsin (32-10k cal a BP) history of pluvials, droughts, and vegetation, with some thoughts on forcings

Proxy Interpretations

Sand as a hydrologic indicator

In Mediterranean climates such as pswUS, the mobilization and transport of sediment, particularly coarse sediment (i.e., sand size), is strongly linked to precipitation-related run-off (Inman and Jenkins, 1999; Farnsworth and Milliman, 2003; Warrick and Mertes, 2009; Covault et al., 2010; Xu et al., 2010; Warrick and Barnard, 2012; Gray et al., 2014; Warrick et al., 2015). Research on the rivers of the pswUS confirms this strong connection to climate at both interannual and multi-decadal timescales. Scaling up, it is reasonable to conclude that hydroclimatic processes control the sediment mobilization signal at centennial to millennial timescales for the study region as well (Romans et al., 2009; Covault et al., 2010). This sediment-climate connection is manifest through increases in river discharge and enhanced coarse sediment mobilization and transport during individual wetter-than-average winters or intervals of wetter-than-average winters associated with changes in the mean climate state (Inman and Jenkins, 1999; Farnsworth and Milliman, 2003; Romans et al., 2009; Covault et al., 2010). Considering these modern studies, Kirby et al. (2010) compared percent sand, Lake Elsinore lake level, San Jacinto River discharge, and the PDO index over the 20th century. Their analysis revealed that small changes in sand content (generally < 15-20 %) shows a positive correlation with the San Jacinto River discharge, Lake Elsinore lake level, and the PDO index. In other words, greater river discharge (and higher lake levels) are associated with higher sand content and vice versa. A similar 20th century comparison between percent sand and river discharge was observed for Zaca Lake, also in the pswUS (Kirby et al., 2014).

From these modern and 20th century studies, we contend that the predominant driver of changes in coarse sediment in pswUS lakes is hydroclimate, particularly winter season precipitation variability linked to overall winter wetness. Therefore, we interpret higher percent total sand as reflecting greater precipitation-related runoff (i.e., intensity and/or storm duration) and vice versa. Of course, we cannot assign a specific wetness value to percent sand; however, we can use changes in percent sand as a scaling tool for relative changes in wetness. In other words, higher percent sand content is interpreted to reflect relatively wetter conditions and vice versa for lower percent sand.

Therefore, throughout the discussion below, we use low percent sand values to infer intervals of diminished runoff and thus drier climates and vice versa for high percent sand (Figure 4) (Kirby et al., 2010, 2013, 2014). Our interpretation, however, of the sand data is based on small changes in ambient, or background level, sand – values that range between 0 and 20 percent total sand, generally (Figure 3, 4, and S1). Notably, there are no visible sandy or sandy silt layers within the core sections that are characterized by small changes in sand (SRSD 1-7, 9-14). Instead, the sand is disseminated within the matrix, even within the laminated sections. These small changes in background sand are interpreted to reflect variations in available runoff energy required for the mobilization and transportation of sand into the lake's deepest basin. A depositional model for this process is detailed in Kirby et al. (2010). The glacial sand unit (SRSD 8: 27.6-25.6k cal a BP), however, represents (and requires) an entirely different depositional process and environment. Total sand values during SRSD 8 average 35.4 % ± 17.7, with maximum values exceeding 70 % (Figure 3 and S1). We do not interpret this interval as a period of enhanced run-off. Rather, we suggest (as discussed below) that SRSD 8 reflects a sustained interval of low lake levels (drought) wherein the lake's mud depth boundary, or the depth at which accumulation exceeds erosion, migrated basinward.

As suggested by the high sand content in SRSD 8, other processes can govern the amount of coarse sediment content in lake basins. For example, the gradual lakeward progradation or landward retreat of the mud depth boundary in response to gradual and sustained lake level regressions or transgressions, respectively, can produce dramatic changes in coarse sediment content over time (Dearing, 1997; Pribyl and Shuman, 2014; Shuman and Serravezza, 2017). In other words, as lake level progressively drops, the mud depth boundary migrates basinward. The result of this migration is a progressive coarsening of sediment basinward. Sediments above the mud depth boundary are typically both visually and analytically different than sediments below the mud depth boundary (Shuman, 2003; Anderson et al., 2001, 2008; Shuman et al., 2009). Therefore, it is possible to determine the sediment's depositional environment – deep lake or shallow lake – using standard sedimentological analyses, such as grain size distributions. Moreover, if these sediment data are coupled with additional climate indicators (such as pollen), the interpretation becomes more robust.

To explore the differences between sediment type and depositional environment, first we examined the modern relationship between lake water depth and sand content (Figure 5). As expected, sand content decreases with increasing depth. This relationship between lake depth and sediment size is well known and largely a product of sediment focusing and wave energy dissipation with increasing depth (Davis and Ford, 1982; Hilton, 1985; Blais and Kalff, 1995; Anderson et al., 2001, 2008; Shuman et al., 2009). For modern Lake Elsinore, we can estimate the mud depth based on where the asymptote flattens on the y-axis (see Figure 5) (Rowan et al., 1992; Anderson et al., 2008). The data show that the mud depth is approximately 7.3 m with an upper and lower estimate of 6.0 m and 7.8 m, respectively (Figure 5). Second, we compare the grain size distribution between modern sediments below the Lake Elsinore mud depth boundary (6.01-7.32 m) and the SRSD intervals (1-7, 9-14), or the intervals characterized by small changes in percent total sand (Figure 4 and 6). Third, we compare modern Lake Elsinore beach sediment to the glacial sand unit, SRSD 8 (Figure 6).

These comparisons show that the SRSD intervals 1-7 and 9-14 are similar to the modern grain size distribution found today in Lake Elsinore, for sediments deeper than the mud depth boundary (Figure 6). Conversely, the modern Lake Elsinore beach grain size distribution is more similar to SRSD 8. Taken together, these data suggest that the depositional environment (and processes) for SRSD intervals 1-7 and 9-14 are similar to those governing sedimentation in modern Lake Elsinore below the mud depth boundary (deep lake). SRSD 8, however, is more akin to the depositional environment (and processes) governing sedimentation in modern Lake Elsinore above the mud depth boundary (shallow lake).

In conclusion, we contend that SRSD intervals 1-7 and 9-14 represent changes in precipitation-related runoff dynamics, resulting in small changes (generally < 15-20 %) in ambient, or background, sand content. This conclusion fits with that observed in modern Lake Elsinore over the 20th century as well as modern river process studies (Inman and Jenkins, 1999; Farnsworth and Milliman, 2003; Warrick and Mertes, 2009; Covault et al., 2010; Kirby et al., 2010, 2014; Xu et al., 2010; Warrick and Barnard, 2012; Gray et al., 2014; Warrick et al., 2015). We argue that it is less likely that these small changes in sand reflect the rapid migration of mud-depth boundary. In fact, over the 20th century, Lake Elsinore lake level and percent total sand show a positive correlation, the exact opposite of that expected if the sand reflected the rapid migration of the mud-depth boundary (Kirby et al., 2010).

As an additional and independent assessment of this runoff versus mud depth explanation, we compare the sand content in Lake Elsinore between the Holocene and glacial. Sand content in the Holocene record is very low (avg. 3.3 %), much lower on average than at almost any time in the glacial (Figure 4) (Kirby et al., 2010, 2013, this paper). It is known that the Holocene was drier than the glacial in the pswUS (King, 1976; Heusser, 1978; Enzel et al., 1992; Mensing, 2001; Wells et al., 2003; Anderson et al., 2010; Kirby et al., 2013). If we can assume that average lake depth also decreased in the Holocene in response to this change to a drier climate state, we might expect to see an increase in sand as the mud depth boundary migrated basinward. Conversely, if we assume the glacial was wetter and lake levels were generally higher than today (as research suggests), we should see a decrease in sand content as the mud depth boundary migrates away from the basin. In fact, we observe the exact opposite for the both the Holocene (less sand) and the glacial (more sand). Therefore, we argue that the small changes in ambient, or background, sand content between the Holocene and glacial predominantly reflect changes in precipitation-related runoff (drier Holocene = less runoff and wetter glacial = more runoff).

What about SRSD 8? The grain size distribution as well as total sand content SRSD 8 are clearly different than SRSD 1-7 and 9-14, or the modern sediments below the mud depth boundary (Figure 6). However, the distribution of sediment is quite similar to modern Lake Elsinore beach sediment, or sediment above the mud depth boundary. Consequently, we conclude that SRSD 8 reflects a unique sedimentary response to prolonged and sustained glacial drying, during which the mud depth boundary prograded basinward causing the progressive coarsening of sediment. More details pertaining to SRSD 8 are discussed below.

Pollen as an ecological tracer

The pollen data from core LEDC10-1 were originally reported and interpreted by Heusser et al. (2015). Here, we revisit the pollen data, adding the sediment data, specifically grain size, for a more complete evaluation of the hydrologic-ecologic system (Figure 8). Importantly, because both the pollen and the sediment data were extracted from the same core using the same chronology, we can exam the relationships between hydrologic and ecologic indicators (Hughen et al. 2004; Jennerjahn et al., 2004).

For this study, we plot the same five pollen types as determined by Principal Component Analysis in Heusser et al. (2015) as reflecting the dominant and most straightforward ecological interpretations. These pollen types include: Amaranthaceae, Asteraceae, Quercus, Pinus, and Juniperus-type (Cupressaceae) (Figure 8). To this five, we add Cyperaceae. Changes in Cyperaceae, Amaranthaceae, and Asteraceae likely reflect vegetation growing within the lake's immediate vicinity. Specifically, they are interpreted to reflect changes in extent of the lake's littoral zone and/or herbaceous and halophytic/semi-arid scrub vegetation. For example, higher values of these three pollen types reflect an expanded littoral zone and an increase in herbaceous and halophytic/semi-arid scrub vegetation, fitting with a shallower lake during a drier climate. Lower values of these pollen reflect a deeper lake during a wetter climate (Figure 8).

To characterize the vegetation beyond the lake's immediate vicinity, we focus on three tree genera including Quercus, Pinus, and Juniperus-type (Cupressaceae). In general, lower values of Quercus and higher values of Pinus and Juniperus-type (Cupressaceae) suggest wetter and/or colder conditions. Digging deeper into the tree pollen data and asking the question, "Does a certain genus reflect temperature or moisture more prominently than another," we compared the sand data (i.e., a wetness indicator) to the two dominant and most variable tree genera found in the glacial record: Pinus and Juniperus-type (Cupressaceae) (Figure 8). This simple comparison shows that the sand and Pinus data change similarly over centennial to millennial timescales, except where they diverge strongly in the Holocene (SRSD 1: 12.8-10.1k cal a BP). Based on this similarity, we suggest that glacial Pinus predominantly reflects changes in moisture availability, like the sand data. Juniperus-type (Cupressaceae), however, diverges on several occasions from both the sand and Pinus data (Figure 8). As a result, we suggest that the Juniperus-type (Cupressaceae) data reflect a more complex response to temperature and moisture than the Pinus, perhaps reflecting Juniperus-type's (Cupressaceae) resistance to drought stress (Willson et al., 2008). The divergence of the Juniperus-type (Cupressaceae) pollen from the moisture sensitive Pinus and sand suggest that temperature may be more important to controlling the abundance of Juniperus-type (Cupressaceae) than moisture during the glacial. Albeit a simple interpretation, this compartmentalization of the Pinus and Juniperus-type (Cupressaceae) into moisture and temperature indicators, respectively, allows us to examine relative changes in moisture (sand and Pinus) and temperature (Juniperus-type) through time.

Below, the Lake Elsinore record is discussed from oldest to youngest in the context of the SRSD intervals. The paper is not meant to serve as a comprehensive regional site-to-site comparison, such as that from Kirby et al. (2013), Ibarra et al. (2014), Reheis et al. (2015), or Rosenthal et al. (2017). Rather than repeat that information here, we aim to present the complete 32-10k cal a BP Elsinore sediment and pollen data as they inform on the local history of pluvials, droughts, and vegetation in the pswUS. The only exception to this site-specific focus is a brief regional comparison for the glacial sand interval (SRSD 8, 27.6-25.7k cal a BP).

MIS 3/2 transition: an unsettled climate regime (SRSD 14-7: 32.3-24.9k cal a BP)

The longest period of large amplitude, sustained hydrologic and ecologic variability in the record occurs between SRSD 14-7 (Figure 3, 4, and 8). This period encompasses the MIS 3/2 transition at ca. 29k cal a BP. Sedimentologically, these intervals are characterized by a variety of sediment types, ranging from massive sands (SRSD 8) to discontinuously-laminated sediments with large black organic-rich blebs (Figure 3). Magnetic susceptibility is highly variable as well, indicating changes in sediment provenance, changes in the flux of magnetic minerals into the basin, and/or changes in the preservation of magnetic minerals. Except for a brief interval between 31-30.4k cal a BP, total organic matter is uniformly low, suggesting limited primary productivity and/or poor organic matter preservation. The absence of discrete organic materials for radiocarbon dating throughout most of these intervals supports the latter interpretation. Total carbonate is at or near the lower limit of reliable detection (~4 %) for these intervals (Dean, 1974), suggesting either a lack of carbonate production or carbonate preservation. The pollen data indicate a highly dynamic ecologic system characterized by changes in aquatic littoral zone and herbaceous and halophytic/semi-arid scrub vegetation (Figure 8). Together, these pollen data suggest lake surface contractions and expansions. At the same time, the sand data show considerable large amplitude variability, suggesting changes in winter precipitation related runoff (Figure 8). Within this unsettled climate regime, SRSD 14 (32.3-30.6k cal a BP), 9 (28.4-27.6k cal a BP), and SRSD 8 stand out. SRSD 8 is discussed separately below. SRSD 14 and 9 are interpreted to represent intervals of diminished runoff (low sand), less available moisture (reduced Pinus), and colder conditions (abundant Juniperus-type (Cupressaceae)). Taken together, we interpret SRSD 14 and 9 as cold but dry climate intervals. Small increases in Cyperaceae and herbaceous vegetation suggest an increase in the aerial extent of the littoral zone during SRSD 14 and 9, as expected during a drier climate.

A closer look at the SRSD 8 (27.6-25.7k cal a BP): a glacial mega-drought?

The pollen data indicate a fundamental change in the lake's watershed ecology during SRSD 8 (Figure 8) (Heusser et al., 2015). Pinus decreased while Quercus shows a small increase, together indicating less total moisture. Juniperus-type (Cupressaceae) also decreased interpreted to reflect warmer conditions, perhaps characterized by more evaporation and/or less available soil moisture. The aquatic and herbaceous and halophytic/semi-arid scrub vegetation (Cyperaceae, Amaranthaceae, and Asteraceae) thrived suggesting a significant contraction of the lake's surface area while simultaneously increasing the breadth of the littoral zone. These observations resulted in the glacial mega-drought hypothesis proposed by Heusser et al. (2015). At the same time, the lake basin's sedimentology changed substantially with a significant increase in total sand content (Figure 8). Combining the pollen and sediment data, we interpret SRSD 8 as reflecting a prolonged period of drier-than-average climate. This long term drying allowed the gradual, but sustained progradation of coarse sediment found above the mud depth boundary to migrate basinward. The result is a coarse-grained sediment unit similar to modern Lake Elsinore beach sediment (Figure 6).

This conclusion begs the question, "How shallow was Lake Elsinore during this glacial mega-drought? And, Did the lake desiccate?" Interestingly, there is no evidence for desiccation during SRSD 8, either in the form of mud cracks, root casts, or erosional surfaces. So, if the lake did not desiccate, can we estimate it paleo depth? To answer this question, we explored the modern relationship between lake water depth and grain size distribution, specifically sand content (Figure 5). As expected, sand content decreases with increasing lake water depth. As discussed above, the modern mud depth in Lake Elsinore is approximately 7.3 m with an upper and lower estimate of 6.0 m and 7.8 m, respectively (Figure 5). This estimation does not rule out a much deeper lake, especially during pluvials; it merely provides an upper boundary on minimum lake depth at any given point in time. Using the same sand-depth relationship, we can also estimate the depth during SRSD 8. Averaging the depth and range for percent total sand during SRSD 8 provides an average depth estimation of 3.7 m with an upper boundary of 3.2 m and a lower boundary of 4.5 m (Figure 5), clearly above the modern mud depth boundary.

Using this modern lake water depth-sand relationship, we conclude that Lake Elsinore likely remained a shallow, perennial lake throughout the duration of the glacial mega-drought, despite evidence for a large decrease in available moisture as per the pollen data. The transition to peak sand percent during SRSD 8 is also gradual, suggesting that a progressive and/or sustained drying allowed the gradual, but persistent progradation of mud depth boundary into the deeper lake environment. Finally, the combined sand and pollen data during SRSD 8 indicate that this ~2000-year glacial mega-drought was more severe than other identified glacial droughts in our record, such as SRSD 9 and 14. In the following section, we explore whether or not this nearly ~2000-year glacial mega-drought was regionally pervasive or simply a localized phenomenon?

Glacial mega-drought regional comparisons

Well-dated, continuous, high-resolution terrestrial records spanning MIS 3 and 2 are relatively uncommon in the pswUS. However, there are two records with adequate dating, resolution, and proxy sensitivity that we will examine in the context of the Elsinore glacial mega-drought (SRSD 8): Baldwin Lake (Glover, 2016; Glover et al., 2017) and Lake Manix (Reheis et al., 2015) (Figure 1).

Baldwin Lake in the San Bernardino Mountains (84km northeast of Elsinore and 1680 m higher elevation) contains a 125k cal a BP record (Glover et al., 2017). Pollen data from Baldwin Lake show an increase in xeric flora approximately coeval to the glacial mega-drought inferred at Elsinore (Glover, 2016). This result indicates a similar ecological response to the drought across elevational gradients within the immediate vicinity of the study site.

180 km northeast of Elsinore is a well-dated, continuous record of lake elevation for Lake Manix spanning 45-25k cal a BP (Reheis et al., 2015). Although seemingly distal to Elsinore, Lake Manix was fed by the Mojave River, which drains the San Bernardino Mountains, in which Baldwin Lake is located (Figure 1). These mountains are located <50 km north of the San Jacinto Mountains, the predominant water source for Lake Elsinore. Consequently, it is reasonable to expect that both Lake Elsinore and Lake Manix record similar hydroclimatic signals, despite their large physical separation (Figure 1). The major difference between the two archives is that Lake Manix was located within the heart of the Mojave Desert. Although its source was predominantly the high elevation San Bernardino’s, the Mojave River (the major influent to Lake

Manix) was required to traverse the arid and highly evaporative Mojave Desert. Consequently, transmission of the high elevation hydroclimatic signal from source-to-sink may have experienced more evaporative attenuation than for Lake Elsinore, even under colder (less evaporative) glacial conditions (Enzel, 1992). Recognizing this potential caveat, we compare our results to the Lake Manix lake elevation reconstruction (Figure 8).

The temporal relationship between the Lake Manix lake elevation reconstruction and the Lake Elsinore hydrologic and ecologic data is intriguing (Figure 8). Considering age control issues (see below) both for Elsinore and Manix, we contend that the Manix lowstand between highstands P6 and P7 correlates to the Elsinore glacial mega-drought (SRSD 8). There is an age offset between the two sites; however, age control issues might explain this discrepancy. First, age control points for Lake Elsinore are absent between 30.7 and 26.5k cal a BP, due to a lack of discrete organic materials (Figure 3), thus our attempt at IRSL dating. Consequently, age control for this interval is based entirely on the age model for Lake Elsinore. Second, as Reheis et al. (2015) acknowledges, most age control for Lake Manix is based on biogenic carbonate from bivalves or gastropods. The reservoir age for Lake Manix likely varied through time, particularly between the Holocene and glacial. However, Reheis et al. (2015) use a standard reservoir correction of 140 years as determined by Owen et al. (2007) and Miller et al. (2010) using late Holocene paired shell-charcoal ages. As a result, the aquatic fauna based carbon dates used by Reheis et al. (2015) for the glacial are likely different than reported due to an unknown glacial reservoir effect. Together, these two site age limitations provide some flexibility in the correlation between the two sites. Because the two sites reflect similar high elevation coastal moisture sources, we argue that it is likely that the two records reflect the same hydroclimatic phenomenon. Alternatively, some of this temporal offset may represent differences caused by varying signal transmission between the much larger, evaporative Lake Manix and the much smaller Lake Elsinore. Either way, we contend that there is regional evidence in the pswUS experienced a nearly 2000-year glacial mega-drought during the early part of MIS 2.

Certainly, the discovery of a 2000-yr mega-drought in the middle of the last glacial is cause for discussion. Do these glacial mega-droughts characterize the entire glacial? What ocean-atmosphere conditions are required to create such as sustained period of aridity? What do these conditions tell us about climate change and/or non-linear responses to forcings? How are the conditions required for glacial mega-droughts the same or different than the mega-droughts of Holocene? Finally, how will these conditions be modulated by present global warming? There remains much work to characterize and explain the occurrence of mega-droughts during the last glacial.

The Last Glacial Maximum (LGM) (SRSDs 7-5, 25.7-19.7k cal a BP)

According to Clark et al. (2012), the global LGM is between 26.5-19k cal a BP. Regionally, the LGM may or may not encompass the entirety, or any, of this interval, depending on how one defines the local LGM (LLGM). In the western United States, for example, there is considerable age range variability for the LLGM depending on the climate archive used (e.g., moraines vs. lake sediments vs. marine sediments) (Laabs et al., 2013; Licciardi and Pierce, 2008; Lyle et al., 2012; Menking et al., 2004; Munroe and Laabs, 2013; Munroe et al., 2006; Pak et al., 2012; Rood et al., 2011; Thackray, 2008). Often, for modelling purposes, the LGM is generally defined (and reported) as a singular time slice centered on 21ka, which makes it difficult to compare to time series data (Chiang et al., 2003; Braconnot et al., 2007; Oster et al., 2015; Lora et al., 2017). For Lake Elsinore, we focus on SRSDs 7-5 as the LGM interval. Ostensibly, this determination is somewhat arbitrary. Our rationale, however, for selecting this time interval was to choose an interval that: 1) falls within the timing of the global LGM; 2) is not biased by what we expect to find (e.g., cold and wet); and, 3) does not include the SRSD 8 glacial mega drought interval.

Using these criteria, the LGM encompasses an interval characterized by variable sedimentology, variable run-off, and variable-to-stable vegetation (Figure 3 and 8). The sedimentology includes: 1) massive clay-rich sediment (SRSD 7: 25.7-24.9k cal a BP); 2) variable thickness laminated sediments with large black organic-rich blebs (older half of SRSD 6: 24.9-23.3k cal a BP); 3) discontinuously-laminated organic-rich sediments (younger half of SRSD 6 and the very beginning of SRSD 5); and, 4) variably thick laminated sediments (SRSD 5: 23.3-19.7k cal a BP) (Figure 3). Magnetic susceptibility is variable, indicating changes in sediment provenance, changes in the flux of magnetic minerals into the basin, and/or changes in the preservation of magnetic minerals. Total organic matter is uniformly low except between 25.2-22.9k cal a BP, correlative to the large black organic-rich blebs unit and subsequent discontinuously-laminated unit. Total carbonate increases slightly during the same interval of higher organic matter, suggesting a possible productivity link or an increase in the flux of terrestrial organic detritus. Sand content is higher during SRSD 7 and 6 than during SRSD 5, suggesting a change from more to less runoff throughout the LGM. However, the presence of laminae, even discontinuous laminae, (except during SRSD 7) suggest a deeper, stable lake wherein the core location was below the mud depth boundary and/or the hypolimnion was anoxic. Asteraceae and Amaranthaceae are uniformly low during SRSD 7-5, indicating reduced herbaceous and halophytic/semi-arid scrub vegetation, particularly by comparison to the preceding dry SRSD 8 interval. Together, the pollen data suggest a deeper, stable lake as well. Cyperaceae, however, show a decrease from SRSD 7 through 6, before stabilizing at low values in SRSD 5. The Cyperaceae results suggest a gradual reduction in the extent of the lake's littoral zone from SRSD 7 to 6, culminating in a stable, deep lake by SRSD 5. Quercus and Pinus are relatively invariant throughout SRSDs 7-5 and indicate generally wet conditions. Juniperus-type (Cupressaceae) increase from SRSD 7 through 6 and then stabilize during SRSD 5, suggesting a change from a warmer to cooler climate.

Although the LGM is presented here as encompassing three SRSD intervals, it is only during SRSD 5 that, taken together, the sediment and pollen data obtain relative stability for a 3000-year period. As a result, we suggest that SRSD 5 represent peak LGM conditions locally, or the LLGM. The sediment and vegetation data, however, suggest somewhat contradictory information during SRSD 5. The sand data suggest less runoff during SRSD 5 and thus a drier climate. We note that although the sand content is low, it is still higher than the Holocene average, indicating wetter-than-Holocene conditions. The sedimentology (i.e., variably laminated) also indicates a deep, stable lake wherein the core location was below the mud depth boundary and/or experienced persistent anoxia. The vegetation data, on the other hand, show little to no variability and suggest a perennial lake with a reduced littoral zone and less herbaceous and halophytic/semi-arid scrub vegetation – conditions associated with a wet climate (Figure 8). Notably, the Juniperus-type (Cupressaceae) indicate peak cooling during SRSD 5.

Combining these results, we suggest that SRSD 5 was wet, as compared to the Holocene and SRSD 8, but less wet than during the subsequent SRSD intervals 4 and 3 (see below and Kirby et al., 2013). Consequently, total winter precipitation runoff diminished as per the decrease in sand content. However, the proliferation and stability of mesic vegetation during an apparently drier LLGM may reflect the LLGM's colder climate (as per the Juniperus-type (Cupressaceae) data) rather than wetter. A colder climate could sustain and promote mesic vegetation, even under conditions of less moisture, if – for example – soil moisture is retained in response to cooler, less evaporative conditions. Cooler, less evaporative conditions may also favor the preservation of a deep lake, even during a period of reduced total precipitation and runoff. In fact, the role cooler glacial temperatures and reduced evaporation played in the development and permanence of large glacial lakes in presently arid environments (e.g. the US Great Basin) is well known (*cf.* Ibarra et al., 2014). This cooler, less evaporative and "drier" LLGM scenario is presented as a possible resolution to this apparent conflict between the sedimentology and the pollen during SRSD 5. Additional, well-dated, and continuous regional records encompassing these intervals are required to evaluate this LLGM hypothesis.

Late glacial (SRSD 4 & 3: 19.7-14.4k cal a BP) (Kirby et al., 2013)

Using the sand/runoff interpretation, intervals 4 and 3 represent the longest period of greater precipitation-related runoff intensity and/or storm duration observed between 32-10k cal a BP (Figure 4 and 8). As previously noted in Kirby et al. (2013), these intervals encapsulate Heinrich stadial-1 (19-16k cal a BP), a generally cooler period in the Northern Hemisphere (Kindler et al., 2014). In general, the pollen data agree with the runoff indicators, suggesting the presence of a perennial lake with a reduced littoral zone (less Cyperaceae) and less herbaceous and halophytic/semi-arid scrub vegetation (less Amaranthaceae and Asteraceae). The tree pollen data (less Quercus, more Pinus, more Juniperus-type (Cupressaceae)) also indicate a wetter and cooler period. A closer look at the data show that sand increases slightly from the beginning of SRSD 4 (19.7-18.2k cal a BP), peaking during the latter half of SRSD 3 (18.2-14.4k cal a BP); the same is true for Pinus. Together, these data suggest a trend towards wetter conditions from SRSD 4 to 3. Our temperature indicator, Juniperus-type (Cupressaceae), also suggest a long-term trend from cooler to warmer at the beginning of SRSD 4 through SRSD 3.

Late glacial to Holocene transition including the Younger Dryas chronozone (SRSD 2-1: 14.4-10.1k cal a BP) (Kirby et al., 2013)

The late glacial to Holocene transition features prominently as a period of large hydrologic and ecologic variability (Figure 8). Kirby et al. (2013) details the proposed forcings driving with these changes (i.e., ice sheet extent, AMOC variability, and changing greenhouse gas concentrations); the details are not repeated here. Sand decreases at the SRSD 3/2 transition (14.4k cal a BP) suggesting a reduction in precipitation related runoff. At the same time, there are decreases in Pinus (drier), Quercus (drier), and Juniperus-type (Cupressaceae) (warmer). Asteraceae and Amaranthaceae increase slightly suggesting an expansion of herbaceous and halophytic/semi-arid scrub vegetation. Finally, Cyperaceae increase as well indicating an expansion of the lake's littoral zone. Taken together, these data indicate a climatic drying and warming from SRSD 3 to SRSD 2 (14.4-12.8k cal a BP) (Figure 8). The transition from SRSD 2 to SRSD 1 (12.8-10.1k cal a BP) is more complex. Sand decreases suggesting yet another reduction in precipitation related runoff. However, there is an increase in Pinus (wetter) and Quercus (wetter) at the same time, lasting about 600 years. Juniperus-type (Cupressaceae) decrease about 200 years before the sand decrease, suggesting near Holocene temperatures by 13.2k cal a BP. Asteraceae and Amaranthaceae generally increase suggesting an additional expansion of herbaceous and halophytic/semi-arid scrub vegetation; although, a brief decrease in Asteraceae correlative to the Pinus increase ca. 13-12.4k cal a BP suggests a possible short-lived lake expansion. Finally, Cyperaceae show no significant change from SRSD 2 to 1, suggesting a stable littoral zone. Taken together, the sediment and vegetation data indicate a complex response at the SRSD 2 to 1 transition (Figure 8). The sedimentology suggests a continued drying trend; whereas, some of the vegetation data (Pinus, Quercus, and Asteraceae) indicate a brief return (~600 years) to wetter and/or cooler conditions. By 12.6-12.4k cal a BP, the data all agree that the climate achieved near Holocene conditions, characterized by drier and warmer climate and a smaller, shallower but stable lake (Figure 8).

Conclusion

In this paper, we present a history of pluvials, droughts, and vegetation in the pswUS spanning 32-10k cal a BP. Increases in percent total sand are interpreted to reflect greater precipitation-related runoff (i.e., intensity and/or storm duration) and vice versa. Although the sand data indicate a range of hydroclimatic variability, the late Wisconsin was wetter than the Holocene, in general. Vegetation, as inferred from pollen, reveal generally wetter and cooler conditions during the late Wisconsin as well. The pollen data also indicate intervals of highly variable ecologic change as well as long intervals of vegetative stability. The interval between 32.3-24.9k cal a BP is the longest period of large amplitude, sustained hydrologic and ecologic variability in the record. Punctuating this interval is a proposed glacial mega-drought (27.6-25.7k cal a BP), wherein Lake Elsinore's surface area and depth diminished extensively and mesic flora declined to near Holocene levels. Although the lake did not desiccate during this interval, lake water depth decreased to ~3.2-4.5 m. A lack of desiccation during this extended glacial mega-drought likely reflects cooler temperatures and a decrease in net annual evaporation, thus maintaining a shallow lake under drier conditions. Under similar conditions in the Holocene, the lake would likely desiccate completely. Coeval increases in xeric vegetation at Baldwin Lake in the San Bernardino Mountains (Glover, 2016; Glover et al., 2017) and a large lake level regression at Lake Manix (Mojave Desert) (Reheis et al., 2015) indicates a coherent regional response and shared climatic forcing. We suggest that the LLGM occurred between 23.3-19.7k cal a BP (SRSD 5) encapsulating a nearly 3000-year interval of relative ecologic and hydrologic stability. We interpret the LLGM as a cooler, less evaporative, and "drier" climate; although, the LLGM was not drier than the Holocene but not as wet as the subsequent intervals SRSD 4 & 3 (19.7-14.4k cal a BP). SRSD intervals 4 and 3 represent the longest period of greater precipitation-related runoff intensity and/or storm duration observed between 32-10k cal a BP. There is evidence for a trend toward wetter and warmer conditions beginning at 19.7k cal a BP and peaking at 14.4k cal a BP. The late glacial to Holocene transition (SRSD 2-1: 14.4-10.1k cal a BP) features prominently as a period of large hydrologic and ecologic variability. In general, SRSD 2 is characterized as an interval of reduced runoff, a warmer climate, and a decrease in lake surface area and depth. The relationship, however, between the hydrologic and ecologic indicators is more complex during the SRSD 2 to 1 transition. The vegetation data (Pinus, Quercus, and Asteraceae) indicate a brief return (~600 years) to wetter conditions between 13-

12.6/12.4k cal a BP; whereas, the hydrologic indicator indicate a continued decrease in runoff. By 12.6-12.4k cal a BP, the ecology and hydrology achieved near Holocene conditions. Future work will examine these results in the context of regional and hemispheric data as well as late Wisconsin climatic forcings.

Acknowledgements

This research was funded by the National Science Foundation (#031511, #0731843, and #1203549) and the American Chemical Society-Petroleum Research Fund (#4187-B8). Special thanks to Mr. Pat Kilroy and the City of Lake Elsinore for lake access; Mr. Joe Holbrook (CSUF) for help opening the cores; Mr. Peter Cattaneo (Syracuse University) for expert advice and service collecting and processing the seismic reflection data. Most importantly, this work would not be possible without the excellent service and research quality cores collected by Mr. John Gregg and Gregg Drilling and Testing, Inc. The authors thank Mr. Daniel Ibarra, Dr. David Miller, one anonymous reviewer, and the editor (Dr. Joe Liccardi) for thoughtful and helpful reviews. Sandy discussions with Dr. Joe Carlin and comments by Dr. Nicole Bonuso are appreciated, too. MEK dedicates this paper to Dr. John T. Andrews for giving me an opportunity.

References

Anderson M, Whiteaker L, Wakefield E, Amrhein C, 2008. Properties and distribution of sediment in the Salton Sea, California: an assessment of predictive models. Hydrobiologia 604, 97-110.

Anderson MA, 2001. Internal loading and nutrient cycling in Lake Elsinore. In. Lake Elsinore: Santa Ana Regional Water Quality Control Board, 52.

Anderson, R.S., Starratt, S., Jass, R.M.B., Pinter, N., 2010. Fire and vegetation history on Santa Rosa Island, Channel Islands, and long-term environmental change in southern California. Journal of Quaternary Science 25, 782-797.

Antevs E, 1948. Climatic Changes and Pre-White Man. The Great Basin, with emphasis on glacial and postglacial times. University of Utah Bulletin 38, 166-91.

Blaauw M, Christen JA, 2011. Flexible paleoclimate age-depth models using an autoregressive gamma process. Bayesian Analysis 6, 457-74.

Blais, J.M., Kalff, J., 1995. The Influence of Lake Morphometry on Sediment Focusing. Limnology and Oceanography 40, 582-588.

Braconnot, P., Otto-Bliesner, B., Harrison, S., Joussaume, S., Peterchmitt, J.Y., Abe-Ouchi, A., Crucifix, M., Driesschaert, E., Fichefet, T., Hewitt, C.D. and Kageyama, M., 2007. Results of PMIP2 coupled simulations of the Mid-Holocene and Last Glacial Maximum–Part 1: experiments and large-scale features. *Climate of the Past*, *3*(2), pp.261-277.

Brito-Castillo L, Douglas AV, Leyva-Contreras A, Lluch-Belda D, 2003. The effect of large-scale circulation on precipitation and streamflow in the Gulf of California continental watershed. International Journal of Climatology 23, 751-68.

Cayan DR, Peterson DH, 1989. The Influence of North Pacific Atmospheric Circulation on Streamflow in the West in Aspects of Climate Variability in the Pacific and the Western Americas. In: Agu, ed. Geophysical Monograph Series. Washington, 375-97. (Union AG, ed. 55.)

Cayan DR, Redmond KT, Riddle RG, 1999. ENSO and hydrologic extremes in the western United States. Journal of Climate 12, 2881-93.

Chiang, J.C., Biasutti, M. and Battisti, D.S., 2003. Sensitivity of the Atlantic intertropical convergence zone to last glacial maximum boundary conditions. *Paleoceanography*, *18*(4).

Clark PU, Shakun JD, Baker PA, et al., 2012. Global climate evolution during the last deglaciation. Proc Natl Acad Sci U S A 109, E1134-42.

Covault J., Romans B., Fildani A, Mcgann M, Graham S., 2010. Rapid Climatic Signal Propagation from Source to Sink in a Southern California Sediment-Routing System. The Journal of Geology 118, 247-59.

Csato I, Kendall CGSC, Nairn AEM, Baum GR, 1997. Sequence stratigraphic interpretations in the southern Dead Sea basin, Israel. Geological Society of America Bulletin 109, 1485-501.

Damiata, B.N. and Lee, T.C., 1986. Geothermal exploration in the vicinity of Lake Elsinore, Southern California. *Geothermal Resource Council Trans*, *10*, pp.119-123.

Davis, M.B., Ford, M.S., 1982. Sediment Focusing in Mirror Lake, New Hampshire. Limnology and Oceanography 27, 137-150.

Dean, W. E. (1974). Determination of carbonate and organic matter in calcareous sedimentary rocks by loss on ignition: Comparison with other methods. *Journal of Sedimentary Petrology, 44*, 242-248.

Dearing, J.A., 1997. Sedimentary indicators of lake-level changes in the humid temperate zone: A critical review. Journal of Paleolimnology 18, 1-14.

Enzel Y, 1992. Flood Frequency of the Mojave River and the Formation of Late Holocene Playa Lakes, Southern California, USA. The Holocene 2, 11-8.

Enzel, Y., Brown, W.J., Anderson, R.Y., Mcfadden, L.D., Wells, S.G., 1992. Short-Duration Holocene Lakes in the Mojave River Drainage-Basin, Southern California. Quaternary Research 38, 60-73.

Enzel Y, Agnon A, Stein M, 2006. New Frontiers in Dead Sea Paleoenvironmental Research. Boulder: Geological Society of America.

Farnsworth, K.L., Milliman, J.D., 2003. Effects of climatic and anthropogenic change on small mountainous rivers: the Salinas River example. Global and Planetary Change 39, 53-64.

Glover, K.C., 2016. Southern California climate and vegetation over the past 125,000 years from lake sequences in the San Bernardino Mountains. Ph.D. Thesis, University of California - Los Angeles, Los Angeles.

Glover KC, Macdonald GM, Kirby ME, et al., 2017. Evidence for orbital and North Atlantic climate forcing in alpine Southern California between 125 and 10 ka from multi-proxy analyses of Baldwin Lake. Quaternary Science Reviews 167, 47-62.

Gray AB, Pasternack GB, Watson EB, Warrick JA, Goñi MA, 2015. Effects of antecedent hydrologic conditions, time dependence, and climate cycles on the suspended sediment load of the Salinas River, California. Journal of Hydrology 525, 632-49.

Gray AB, Warrick JA, Pasternack GB, Watson EB, Goñi MA, 2014. Suspended sediment behavior in a coastal dry-summer subtropical catchment: Effects of hydrologic preconditions. Geomorphology 214, 485-501.

Hanson R, Dettinger M, Newhouse M, 2006. Relations between climatic variability and hydrologic time series from four alluvial basins across the southwestern United States. Hydrogeology Journal 14, 1122-46.

Heusser, L., 1978. Pollen in Santa Barbara Basin, California; a 12,000-yr record. Geological Society of America Bulletin 89, 673-678.

Heusser L, Sirocko F, 1997. Millennial pulsing of environmental change in southern California from the past 24 k.y: A record of Indo-Pacific ENSO events? Geology 25, 243-6.

Heusser LE, 1995. Pollen stratigraphy and paleoecologic interpretation of the 160-k.y. record from Santa Barbara Basin, Hole 893A. In: Kennett JP, Baldauf JG, Lyle M, eds. Proc. ODP, Sci. Results. College Station, TX, 265-79. (146.)

Heusser LE, Kirby ME, Nichols JE, 2015. Pollen-based evidence of extreme drought during the last Glacial (32.6–9.0 ka) in coastal southern California. Quaternary Science Reviews 126, 242-53.

Hiner CA, Kirby ME, Bonuso N, Patterson WP, Palermo J, Silveira E, 2016. Late Holocene hydroclimatic variability linked to Pacific forcing: evidence from Abbott Lake, coastal central California. Journal of Paleolimnology 56, 299-313.

Hudson T, 1978. Lake Elsinore Valley: its story. Lake Elsinore: Mayhall Print Shop.

Hughen KA, Eglinton TI, Xu L, Makou M, 2004. Abrupt tropical vegetation response to rapid climate changes. Science 304, 1955-9.

Hull AG, 1990. Seismotectonics of the Elsinore-Temecula Trough, Elsinore Fault Zone, Southern California. Santa Barbara: UC Santa Barbara, Ph.D.

Hull AG, Nicholson C, 1992. Seismotectonics of the northern Elsinore fault zone, southern California. Bulletin of the Seismological Society of America 82, 800-18.

Ibarra DE, Egger AE, Weaver KL, Harris CR, Maher K, 2014. Rise and fall of late Pleistocene pluvial lakes in response to reduced evaporation and precipitation: Evidence from Lake Surprise, California. Geological Society of America Bulletin, B31014. 1.

Inman DL, Jenkins SA, 1999. Climate change and the episodicity of sediment flux of small California Rivers. Journal of Geology 107, 251-70.

Jennerjahn TC, Ittekkot V, Arz HW, Behling H, Pätzold J, Wefer G, 2004. Asynchronous terrestrial and marine signals of climate change during Heinrich events. Science 306, 2236-9.

Kam J, Sheffield J, 2016. Increased drought and pluvial risk over California due to changing oceanic conditions. Journal of Climate 29, 8269-79.

Kindler P, Guillevic M, Baumgartner M, Schwander J, Landais A, Leuenberger M, 2014. Temperature reconstruction from 10 to 120 kyr b2k from the NGRIP ice core. Climate of the Past 10, 887.

King Jr, T.J., 1976. Late Pleistocene-early Holocene history of coniferous woodlands in the Lucerne Valley region, Mohave Desert, California. Western North American Naturalist 36, 227-238.

Kirby M, Lund S, Anderson M, Bird B, 2007. Insolation forcing of Holocene climate change in Southern California: a sediment study from Lake Elsinore. Journal of Paleolimnology 38, 395-417.

Kirby ME, Feakins SJ, Bonuso N, Fantozzi JM, Hiner CA, 2013. Latest Pleistocene to Holocene hydroclimates from Lake Elsinore, California. Quaternary Science Reviews 76, 1-15.

Kirby ME, Feakins SJ, Hiner CA, et al., 2014. Tropical Pacific forcing of Late-Holocene hydrologic variability in the coastal southwest United States. Quaternary Science Reviews 102, 27-38.

Kirby ME, Lund SP, Patterson WP, et al., 2010. A Holocene record of Pacific Decadal Oscillation (PDO)-related hydrologic variability in Southern California (Lake Elsinore, CA). Journal of Paleolimnology 44, 819-39.

Kirby ME, Lund SP, Poulsen CJ, 2005. Hydrologic variability and the onset of modern El Nino-Southern Oscillation: a 19 250-year record from Lake Elsinore, southern California. Journal of Quaternary Science 20, 239-54.

Kirby ME, Poulsen CJ, Lund SP, Patterson WP, Reidy L, Hammond DE, 2004. Late Holocene lake-level dynamics inferred from magnetic susceptibility and stable oxygen isotope data: Lake Elsinore, Southern California (USA). Journal of Paleolimnology 31, 275-93.

Krummenacher D, Gastil RG, Bushee J, Doupont J, 1975. K-Ar Apparent Ages, Peninsular Ranges Batholith, Southern California and Baja California. Geological Society of America Bulletin 86, 760-8.

Laabs BJC, Munroe JS, Best LC, Caffee MW, 2013. Timing of the last glaciation and subsequent deglaciation in the Ruby Mountains, Great Basin, USA. Earth and Planetary Science Letters 361, 16-25.

Licciardi JM, Pierce KL, 2008. Cosmogenic exposure-age chronologies of Pinedale and Bull Lake glaciations in greater Yellowstone and the Teton Range, USA. Quaternary Science Reviews 27, 814-31.

Löfverström M, Caballero R, Nilsson J, Kleman J, 2014. Evolution of the large-scale atmospheric circulation in response to changing ice sheets over the last glacial cycle. Climate of the Past 10, 1453-71.

Lora, J.M., Mitchell, J.L., Tripati, A.E., 2016. Abrupt reorganization of North Pacific and western North American climate during the last deglaciation. Geophysical Research Letters 43, 11796-11804.

Lora JM, Mitchell JL, Risi C, Tripati AE, 2017. North Pacific atmospheric rivers and their influence on western North America at the Last Glacial Maximum. Geophysical Research Letters.

Lyle M, Heusser L, Ravelo C, et al., 2012. Out of the tropics: the Pacific, Great Basin lakes, and late Pleistocene water cycle in the western United States. Science 337, 1629-33.

Lynch HB, 1931. Rainfall and stream run-off in Southern California since 1769. In. Los Angeles: The Metropolitan Water District of Southern California, 31.

Mann J, J.F., 1956. The origin of Elsinore Lake Basin. Bulletin of the Southern California Academy of Sciences 55, 72-8.

Masi GJ. Orographic and large-scale influence on Southern California precipitation patterns. Proceedings of the Sixth Conference on Coastal Atmospheric and Oceanic Prediction and Processes, 2005.

Menking KM, Syed KH, Allen BD, Anderson RY, Shafike NG, 2004. Wetter or colder during the Last Glacial Maximum? Revisiting the pluvial lake question in southwestern North America Quaternary Research 62, 280-8.

Mensing, S.A., 2001. Late-Glacial and Early Holocene vegetation and climate change near Owens Lake, eastern California. Quaternary Research 55, 57-65.

Miller, D.M., Schmidt, K.M., Mahan, S.A., McGeehin, J.P., Owen, L.A., Barron, J.A., Lehmkuhl, F. and Löhrer, R., 2010. Holocene landscape response to seasonality of storms in the Mojave Desert. *Quaternary International*, *215*(1), pp.45-61.

Morton D, Miller F. K/Ar apparent ages of plutonic rocks from the northern part of the Peninsular Ranges batholith, southern California. Proceedings of the Geological Society of America Abstracts with Programs, 1987, 435.

Munroe JS, Laabs BJ, Shakun JD, et al., 2006. Latest Pleistocene advance of alpine glaciers in the southwestern Uinta Mountains, Utah, USA: evidence for the influence of local moisture sources. Geology 34, 841-4.

Munroe JS, Laabs BJC, 2013. Temporal correspondence between pluvial lake highstands in the southwestern US and Heinrich Event 1. Journal of Quaternary Science 28, 49-58.

Myers N, Mittermeier RA, 2000. Biodiversity hotspots for conservation priorities. (Cover story). Nature 403, 853.

Neelin JD, Langenbrunner B, Meyerson JE, Hall A, Berg N, 2013. California Winter Precipitation Change under Global Warming in the Coupled Model Intercomparison Project Phase 5 Ensemble. Journal of Climate 26, 6238-56.

Oster JL, Ibarra DE, Winnick MJ, Maher K, 2015. Steering of westerly storms over western North America at the Last Glacial Maximum. Nature Geosci 8, 201-5.

Owen, L.A., Bright, J., Finkel, R.C., Jaiswal, M.K., Kaufman, D.S., Mahan, S., Radtke, U., Schneider, J.S., Sharp, W., Singhvi, A.K. and Warren, C.N., 2007. Numerical dating of a Late Quaternary spit-shoreline complex at the northern end of Silver Lake playa, Mojave Desert, California: A comparison of the applicability of radiocarbon, luminescence, terrestrial cosmogenic nuclide, electron spin resonance, U-series and amino acid racemization methods. *Quaternary International*, *166*(1), pp.87-110.

Pak DK, Lea DW, Kennett JP, 2012. Millennial scale changes in sea surface temperature and ocean circulation in the northeast Pacific, 10–60 kyr BP. Paleoceanography 27.

Pribyl, P., Shuman, B.N., 2014. A computational approach to Quaternary lake-level reconstruction applied in the central Rocky Mountains, Wyoming, USA. Quaternary Research 82, 249-259.

Pyke, B. N., 2013. A holocene hydroclimatic investigation of lake elsinore, southern california, using seismic reflection and sediment core data, MS Thesis, California State University, Fullerton, 96pp.

Reheis MC, Miller DM, Mcgeehin JP, Redwine JR, Oviatt CG, Bright J, 2015. Directly dated MIS 3 lake-level record from Lake Manix, Mojave Desert, California, USA. Quaternary Research 83, 187-203.

Rhodes EJ, 2015. Dating sediments using potassium feldspar single-grain IRSL: Initial methodological considerations. Quaternary International 362, 14-22.

Rodionov S, 2015. A sequential method of detecting abrupt changes in the correlation coefficient and its application to Bering Sea climate. Climate 3, 474-91.

Rodionov, S.N., 2004. A sequential algorithm for testing climate regime shifts. *Geophysical Research Letters*, *31*(9).

Romans BW, Normark WR, Mcgann MM, Covault JA, Graham SA, 2009. Coarse-grained sediment delivery and distribution in the Holocene Santa Monica Basin, California: implications for evaluating source-to-sink flux at millennial time scales. Geological Society of America Bulletin 121, 1394-408.

Rood DH, Burbank DW, Finkel RC, 2011. Chronology of glaciations in the Sierra Nevada, California, from 10Be surface exposure dating. Quaternary Science Reviews 30, 646-61.

Rosenthal, J.S., Meyer, J., Palacios-Fest, M.R., Young, D.C., Ugan, A., Byrd, B.F., Gobalet, K. and Giacomo, J., 2017. Paleohydrology of China Lake basin and the context of early human occupation in the northwestern Mojave Desert, USA. *Quaternary Science Reviews*, *167*, pp.112-139.

Rowan DJ, Kalff J, Rasmussen JB, 1992. Estimating the Mud Deposition Boundary Depth in Lakes from Wave Theory. Canadian Journal of Fisheries and Aquatic Sciences 49, 2490-7.

Scholz, C.A., 2001. Application of seismic sequence stratigraphy in lacustrine basins, in: Last, W.M., Smol, J.P. (Eds.), Tracking Environmental Change Using Lake Sediments. Kluwer Academic Publishers, Dordrecht, pp. 7-22.

Seager R, Ting M, Li C, et al., 2013. Projections of declining surface-water availability for the southwestern United States. Nature Clim. Change 3, 482-6.

Shields CA, Kiehl JT, 2016. Atmospheric river landfall-latitude changes in future climate simulations. Geophysical Research Letters 43, 8775-82.

Shuman, B., 2003. Controls on loss-on-ignition variation in cores from two shallow lakes in the northeastern United States. Journal of Paleolimnology 30, 371-385.

Shuman, B., Henderson, A.K., Colman, S.M., Stone, J.R., Fritz, S.C., Stevens, L.R., Power, M.J., Whitlock, C., 2009. Holocene lake-level trends in the Rocky Mountains, U.S.A. Quaternary Science Reviews 28, 1861-1879.

Shuman, B.N., Serravezza, M., 2017. Patterns of hydroclimatic change in the Rocky Mountains and surrounding regions since the last glacial maximum. Quaternary Science Reviews 173, 58-77.

Silver L, Taylor Jr H, Chappell B. Some petrological, geochemical and geochronological observations of the Peninsular Ranges batholith near the international border of the USA and Mexico, Mesozoic Crystalline Rocks PL Abbott, VR Todd, 83–110, Department of Geological Sciences, San Diego State University, Guideb. for Geol. Proceedings of the Dept. of Geol. Sci., Guidebook for Geological Society of America Annual Meeting, San Diego, Calif, 1979.

Thackray GD, 2008. Varied climatic and topographic influences on Late Pleistocene mountain glaciation in the western United States. Journal of Quaternary Science 23, 671-81.

Thiros, S. A. (1781). Section 12. Conceptual understanding and groundwater quality of the basin-fill aquifers in the Santa Ana Basin, California. *US Geological Survey Professional Paper*, *2010*, 219-65.

Toppozada TR, Parke DL, Higgins CT, 1978. Seismicity of California, 1900-1931. California Division of Mines and Geology.

Vaughan PR, Thorup KM, Rockwell TK, 1999. Paleoseismology of the Elsinore fault at Agua Tibia Mountain, southern California. Bulletin of the Seismological Society of America 89, 1447-57.

Warrick, J.A., Barnard, P.L., 2012. The offshore export of sand during exceptional discharge from California rivers. Geology 40, 787-790.

Warrick JA, Melack JM, Goodridge BM, 2015. Sediment yields from small, steep coastal watersheds of California. Journal of Hydrology: Regional Studies 4, 516-34.

Warrick, J.A., Mertes, L.A.K., 2009. Sediment yield from the tectonically active semiarid Western Transverse Ranges of California. Geological Society of America Bulletin 121, 1054-1070.

Warrick JA, Mertes LA, Washburn L, Siegel DA, 2004. A conceptual model for river water and sediment dispersal in the Santa Barbara Channel, California. Continental Shelf Research 24, 2029-43.

Warrick JA, Rubin DM, 2007. Suspended-sediment rating curve response to urbanization and wildfire, Santa Ana River, California. Journal of Geophysical Research: Earth Surface 112.

Weber Jr F, 1977. Seismic hazards related to geologic factors, Elsinore and Chino fault zones, northwestern Riverside County, California, Calif Div. Div. Mines and Geol., Open-File Report, 77-4.

Wells SG, Brown JB, Enzel Y, Anderson RY, Mcfadden LD, eds, 2003. Late Quaternary geology and paleohydrology of pluvial Lake Mojave, southern California. Boulder, CO: Geological Society of America.

Willson, C.J., Manos, P.S. and Jackson, R.B., 2008. Hydraulic traits are influenced by phylogenetic history in the drought-resistant, invasive genus Juniperus (Cupressaceae). *American Journal of Botany*, *95*(3), pp.299-314.

Wong CI, Potter GL, Montañez IP, Otto-Bliesner BL, Behling P, Oster JL, 2016. Evolution of moisture transport to the western US during the last deglaciation. Geophysical Research Letters 43, 3468-77.

Xu JP, Swarzenski PW, Noble M, Li A-C, 2010. Event-driven sediment flux in Hueneme and Mugu submarine canyons, southern California. Marine Geology 269, 74-88.

Yilmaz, Ö., 2001. *Seismic data analysis: Processing, inversion, and interpretation of seismic data*. Society of exploration geophysicists.

Yoon J-H, Wang SS, Gillies RR, Kravitz B, Hipps L, Rasch PJ, 2015. Increasing water cycle extremes in California and in relation to ENSO cycle under global warming. Nature communications 6.

Figure Captions

Figure 1. A) Study site with bathymetry, core locations, and seismic line locations discussed in the text; B) Regional map with Lake Elsinore and other sites mentioned in the text; C) Seismic

line map. Abbreviations: SJ Mtns = San Jacinto Mountains; SBB = Santa Barbara Basin. Core references: LESS02-8/10 (Kirby et al., 2004, 2005); LEGC03-2/3 (Kirby et al., 2007, 2010); LEDC10-1 (Kirby et al., 2013; Heusser et al., 2015; this paper).

Figure 2. A) LEDC10-1 age versus depth, B) and C) Age model differences between this paper and Kirby et al. (2013) and Heusser et al. (2015).

Figure 3. LEDC10-1 core sediment data. A) Stratigraphic column with enhanced, subjective coloring to highlight variations, B) Magnetic susceptibility, C) Percent total organic matter (LOI 550 °C), D) Percent total carbonate (LOI 950 °C), E) Percent total sand, silt, and clay, F) Percent sand without the glacial sand unit. SRSD intervals are highlighted by dashed grey boxes.

Figure 4. Percent total sand with sequential regime shift detection break-points shown by bold black line. Holocene sand average (3.3 %) from Kirby et al. (2010) is shown as dashed black line. SRSD intervals are highlighted by dashed grey boxes.

Figure 5. Lake bottom sediment percent sand versus lake water depth. The green dashed lines represent the 95% bootstrap confidence intervals for the regression curve.

Figure 6. Lake Elsinore grain size distributions plots: 1) modern Lake Elsinore beach sample (thick blue line); 2) the glacial sand unit SRSD 8 (thick red line); 3) all modern lake bottom samples between 6.01 and 7.32 m (thin grey lines); and 4) SRSD intervals 1-7 and 9-14 (thin green line).

Figure 7. Seismic reflection lines A) LE line 33 and B) LE line 10. Line intersections are shown as well as the position of core LEDC10-1. The black + are processing artifacts.

Figure 8. Sand-pollen plots versus age. Y-axes oriented so that wet and/or cold interpretation is always up. A) Percent total sand vs. percent Juniperus-type (Cupressaceae), B) Percent total sand vs. percent Pinus, C) Percent total sand vs. percent Quercus, D) Percent total sand vs. percent Asteraceae, E) Percent total sand vs. percent Amaranthaceae, and F) Percent total sand vs.

percent Cyperaceae. G) Lake Manix altitude redrawn from Reheis et al. (2015). P5-8 represent Lake Manix highstands from Reheis et al. (2015). The small blue boxes with horizontal error lines represent the weighted means of statistical age groups (Reheis et al., 2015). The SRSD intervals are highlighted as dashed blue boxes. The glacial mega-drought (SRSD 8) is highlighted by a light-yellow box. The LLGM is highlighted by a light grey box.

Supplemental Figure Captions

Figure S1. LEDC10-1 percent sand by size groupings from A) total sand to E) coarse sand. Very coarse sand (1000-2000 μm) is not shown.

Figure S2. The absolute time step between individual grain size and pollen analyses.

Table 1. Age data for core LEDC10-1

Sample #	LEDC10-1 Depth Range (cm)	Average Depth (cm)	Material	ID	$\delta^{13}C$(‰)[a]	C-14 Age (BP) Used in BACON (v2.2)	±	2-Sigma Range	Age (cy BP)
1	1274-1275	1274.5	Gastropods	*N93630	-25	8,655	35	9,541-9,684	9,613
2	1274-1275	1274.5	Gastropods	*N93631	-25	8,710	35	9,548-9,780	9,664
3	1396-1398	1397.0	Bulk	*94679	-25	10,155 (9,450 Res. Corrected #)	46	11,685-12,030	11,858
4	1508-1510	1509.0	Bulk	*94680	-22.9	10,950 (10,240 Res. Corrected #)	46	12,648-12,964	12,806
5	1540-1542	1541.0	Bulk	*94681	-25	11,650 (10,940 Res. Corrected #)	46	13,334-13,691	13,513
6	1618-1620	1619.0	Bulk	*94682	-24.6	12,200 (11,490 Res. Corrected #)	46	13,887-14,202	14,045
7	1683-1685	1684.0	Mixed Discrete	*N95444	-25	12,140	280	13,437-15,067	14,252
8	1710-1711	1710.5	Mixed Discrete	*N95445	-25	12,460	120	14,091-15,090	14,591
9	1723-1725	1724.0	Mixed Discrete (0.035mgC)	^134836	-25	12,190	290	13,470-15,155	14,313
10	1738-1739	1738.5	Mixed Discrete	*N95446	-25	13,420	230	15,390-16,932	16,161
11	1747-1748	1747.5	Charcoal	*N94003	-25	13,260	35	15,578-16,699	16,139
12	1778-1779	1778.5	Wood	*N94004	-25	13,775	35	16,734-17,049	16,892
13	1823-1824	1823.5	Charcoal	*N94005	-25	14,360	30	17,154-17,790	17,472
14	1823-1824	1823.5	Charcoal	*N94243	-25	14,310	30	17,082-17,706	17,394
15	1870-1872	1871.0	Charcoal; Charred Grass (0.073mgC)	^134837	-25	14,740	200	17,460-18,424	17,942
16	1997-1999	1998.0	Seeds	*N94006	-25	16,580	40	19,461-19,936	19,699
17	2019-2020	2019.5	Seeds	*N94007	-25	16,880	40	19,832-20,321	20,077
18	2081-2082	2081.5	Wood	*N94008	-25	17,980	180	20,911-22,128	21,520
19	2198-2199	2198.5	Seeds	*N94010	-25	19,630	40	23,134-23,779	23,457
20	2280-2282	2281.0	Small Twig	^134839	-23.4	20,870	90	24,881-25,516	25,199
21	2292-2293	2292.5	Charcoal	^134840	-24.1	21,370	90	25,510-25,899	25,700
22	2344-2345	2344.5	Charcoal	*N94245	-25	21,025	40	24,940-25,556	25,248
23	2344-2345	2344.5	Charcoal	*N94011	-25	21,120	70	24,834-25,494	25,164
24	2384-2386	2385.0	Charcoal	^118908	-25	22,010	80	26,078-26,843	26,460
25	2425-2427	2426.0	Small Charcoal (0.16mgC)	^134841	-23.9	21,760	210	25,650-26,481	26,061
26	***2438-2453***	***2445.5***	***IRSL method***	UCLA	na	***29,200 α***	***2,000***	na	
27	***2500-2517***	***2508.5***	***IRSL method***	UCLA	na	***31,300 α***	***2,200***	na	
28	2830-2832	2831.0	Charcoal	^118909	-25	25,940	110	30,419-31,016	30,720
29	2860-2861	2860.5	Wood	*150331	-25	26,550	90	30,970-31,262	31,116
30	2860-2861	2860.5	Wood	*150337	-25	26,270	80	30,758-31,179	30,969

[a] $\delta^{13}C$ values are the assumed values according to Stuiver and Polach (1977) when given without decimal places.

[a] $\delta^{13}C$ values measured for the material itself are given with a single decimal place.

[b] CALIB 6.0.1 Program (Stuiver and Reimer, 1986)

* LLNL AMS Results

^ UCI AMS Results

Correction based on paired bulk - discrete samples - see Kirby et al. (2013)

α Not used in the age model

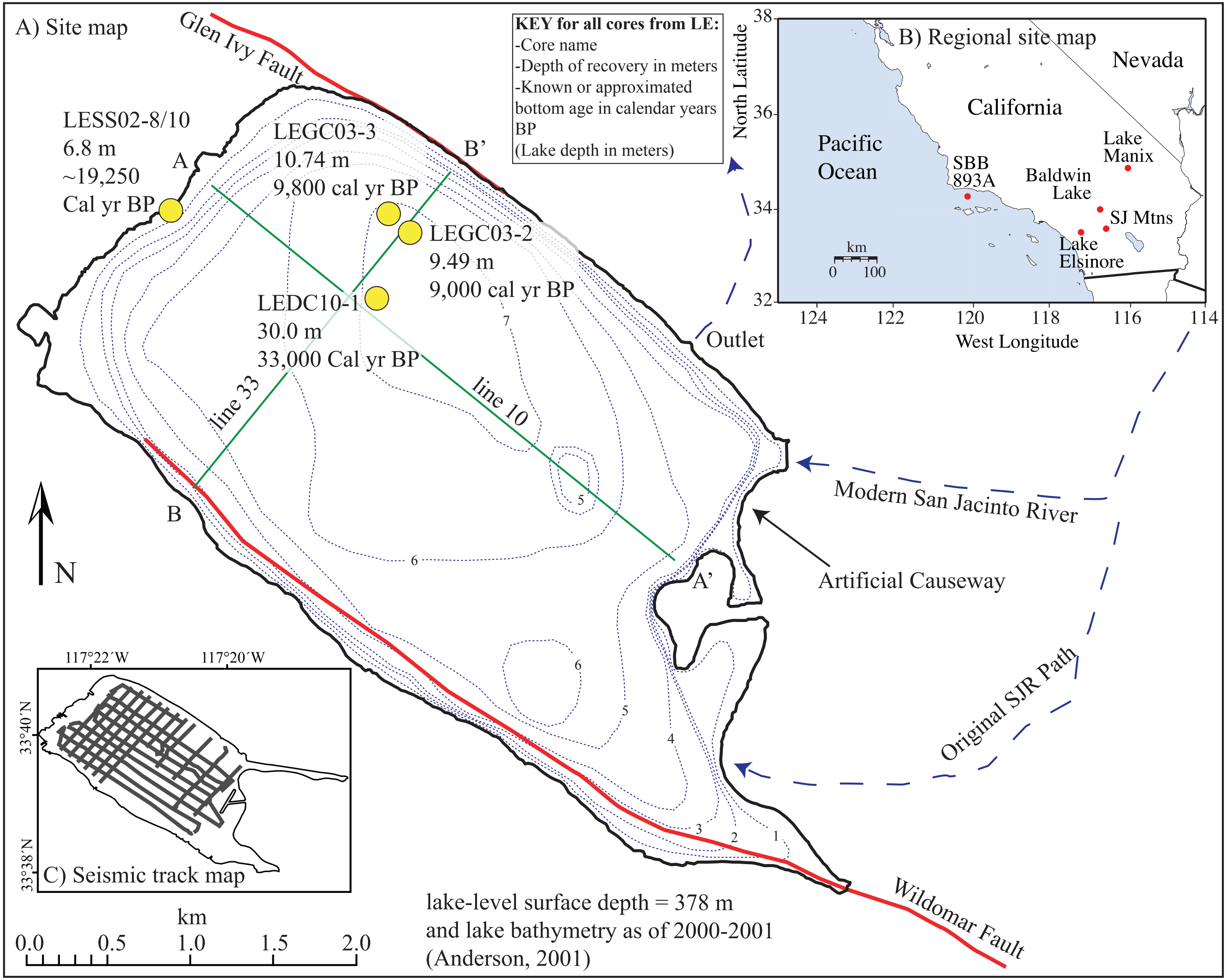
A) Site map
Glen Ivy Fault
KEY for all cores from LE:
-Core name
-Depth of recovery in meters
-Known or approximated bottom age in calendar years BP
(Lake depth in meters)
LESS02-8/10
6.8 m
~19,250
Cal yr BP
A
LEGC03-3
10.74 m
9,800 cal yr BP
B'
LEGC03-2
9.49 m
9,000 cal yr BP
LEDC10-1
30.0 m
33,000 Cal yr BP
line 33
line 10
B
A'
Outlet
7
5
6
6
5
4
3
2
1
N
Modern San Jacinto River
Artificial Causeway
Original SJR Path
Wildomar Fault
B) Regional site map
Nevada
California
Pacific Ocean
SBB 893A
Baldwin Lake
Lake Manix
SJ Mtns
Lake Elsinore
km
0
100
North Latitude
38
36
34
32
124
122
120
118
116
114
West Longitude
C) Seismic track map
117°22´W
117°20´W
33°40´N
33°38´N
km
0.0
0.5
1.0
1.5
2.0
lake-level surface depth = 378 m
and lake bathymetry as of 2000-2001
(Anderson, 2001)

Figure 1

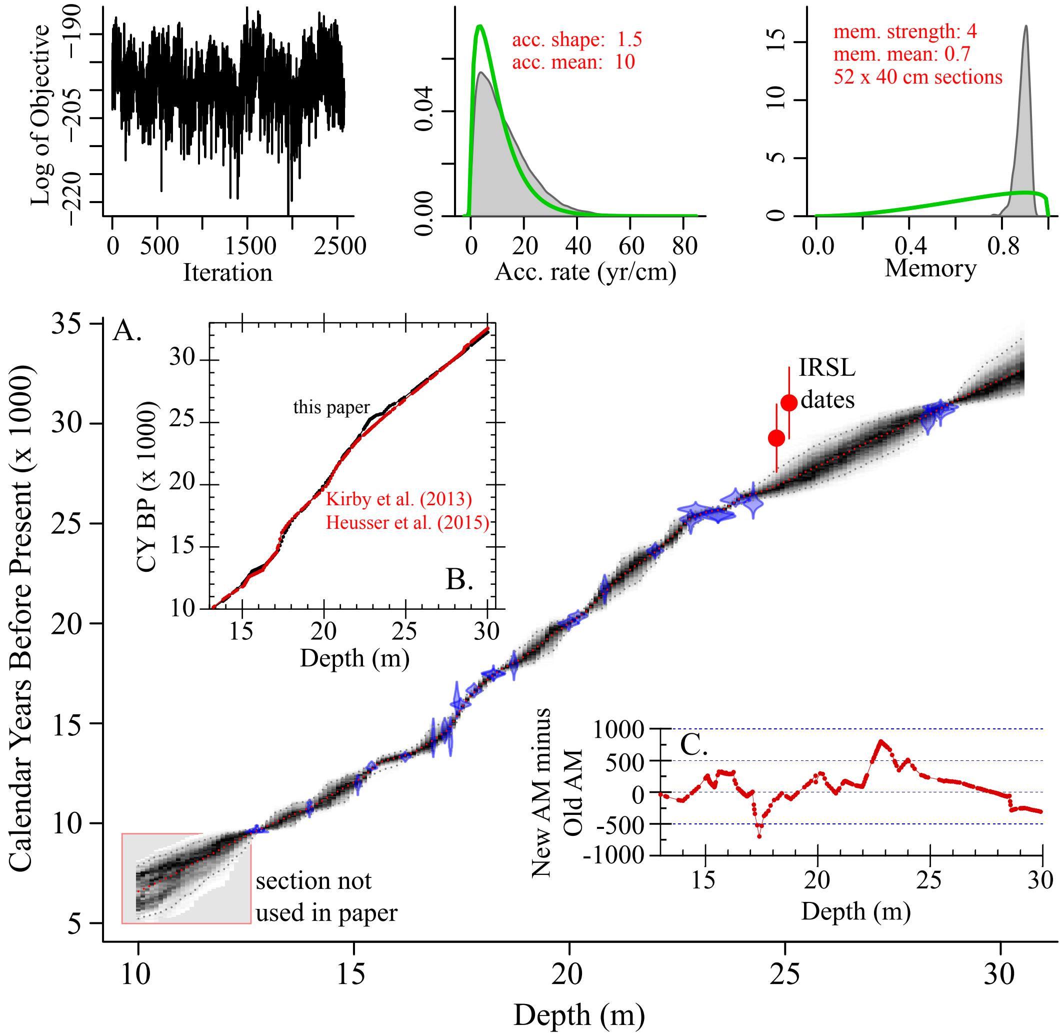
Log of Objective
−190
−205
−220
0
500
1500
2500
Iteration
acc. shape: 1.5
acc. mean: 10
0.00
0.04
0
20
40
60
80
Acc. rate (yr/cm)
mem. strength: 4
mem. mean: 0.7
52 x 40 cm sections
0
5
10
15
0.0
0.4
0.8
Memory
A.
Calendar Years Before Present (x 1000)
35
30
25
20
15
10
5
IRSL
dates
section not
used in paper
10
15
20
25
30
Depth (m)
CY BP (x 1000)
this paper
Kirby et al. (2013)
Heusser et al. (2015)
B.
Depth (m)
C.
New AM minus
Old AM
1000
500
0
-500
-1000
15
20
25
30
Depth (m)

Figure 2

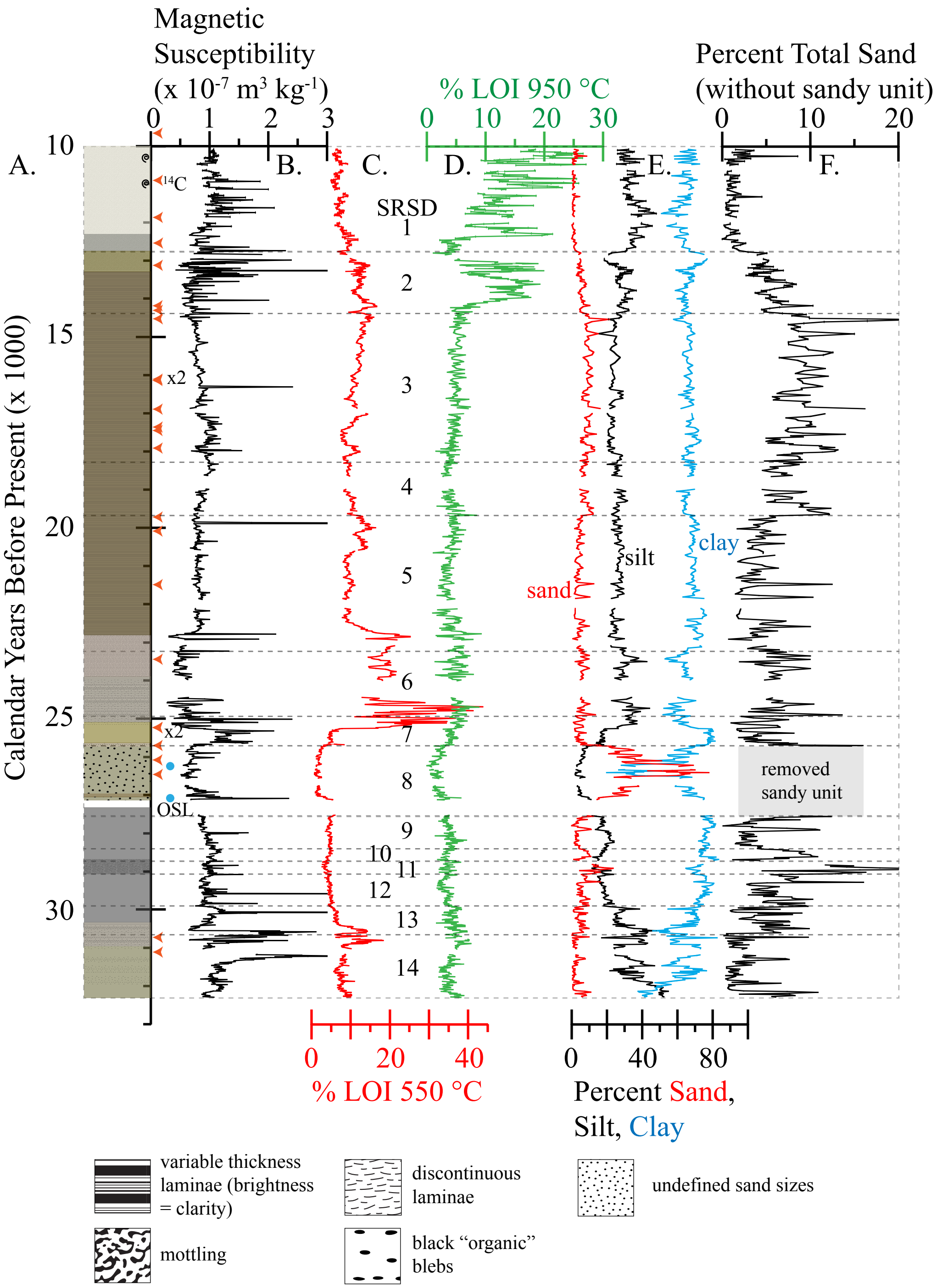
Magnetic Susceptibility (x 10^{-7} m^3 kg^{-1})
0 1 2 3
% LOI 950 °C
0 10 20 30
Percent Total Sand (without sandy unit)
0 10 20
A.
B.
C.
D.
E.
F.
10
15
20
25
30
Calendar Years Before Present (x 1000)
^{14}C
x2
x2
OSL
SRSD
1
2
3
4
5
6
7
8
9
10
11
12
13
14
sand
silt
clay
removed sandy unit
0 20 40
% LOI 550 °C
0 40 80
Percent Sand, Silt, Clay
variable thickness laminae (brightness = clarity)
discontinuous laminae
undefined sand sizes
mottling
black "organic" blebs

Figure 3

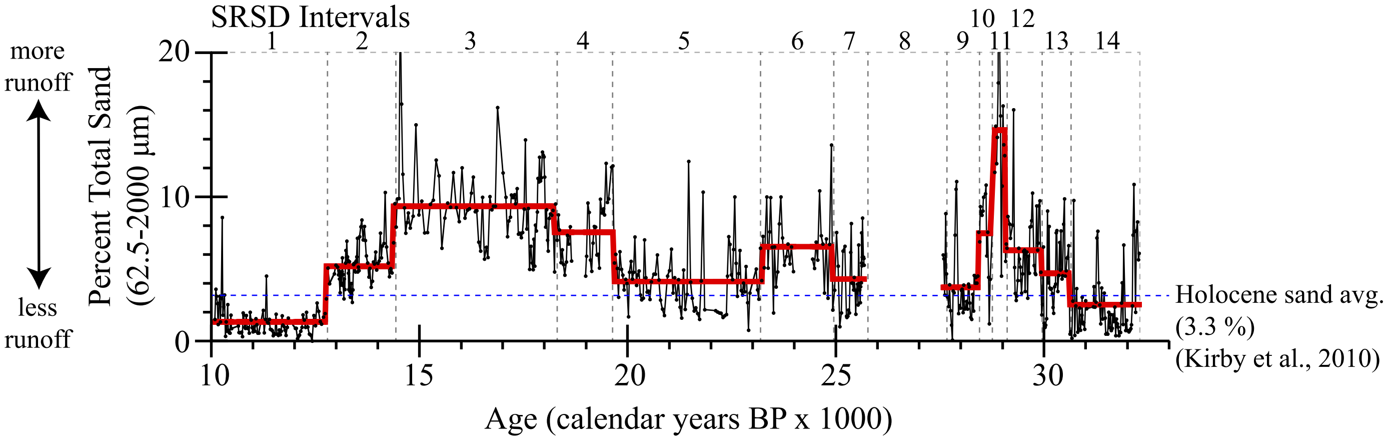
SRSD Intervals
1
2
3
4
5
6
7
8
9
10
11
12
13
14
more runoff
less runoff
Percent Total Sand (62.5-2000 µm)
20
10
0
10
15
20
25
30
Age (calendar years BP x 1000)
Holocene sand avg. (3.3 %) (Kirby et al., 2010)

Figure 4

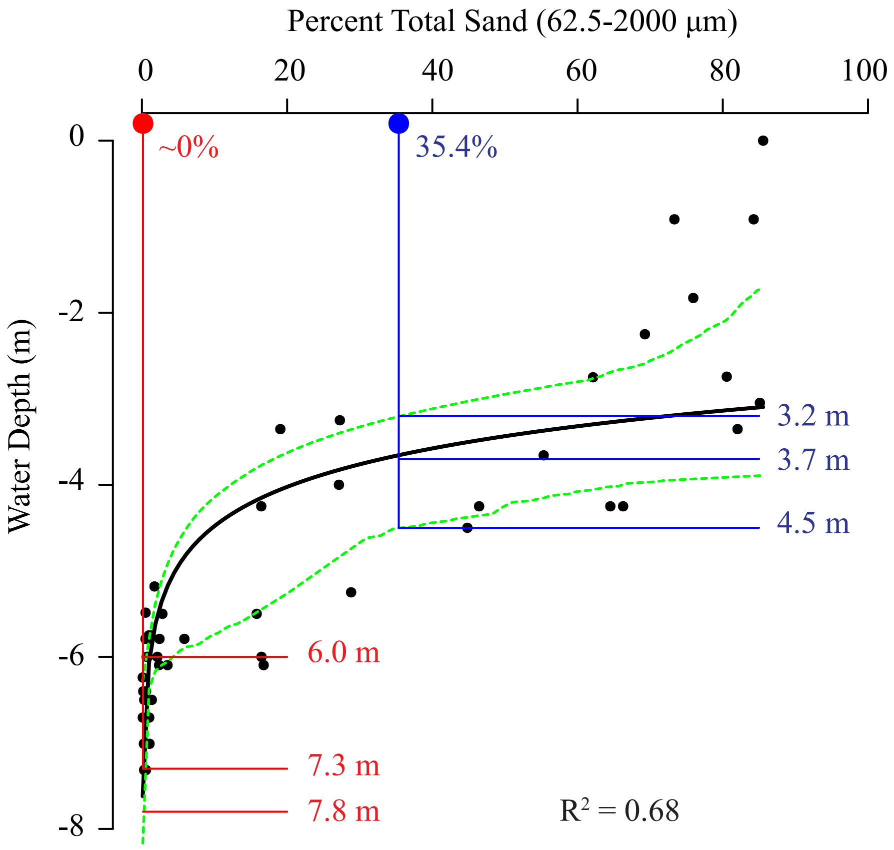
Percent Total Sand (62.5-2000 μm)
0
20
40
60
80
100
Water Depth (m)
0
-2
-4
-6
-8
~0%
35.4%
3.2 m
3.7 m
4.5 m
6.0 m
7.3 m
7.8 m
R² = 0.68

Figure 5

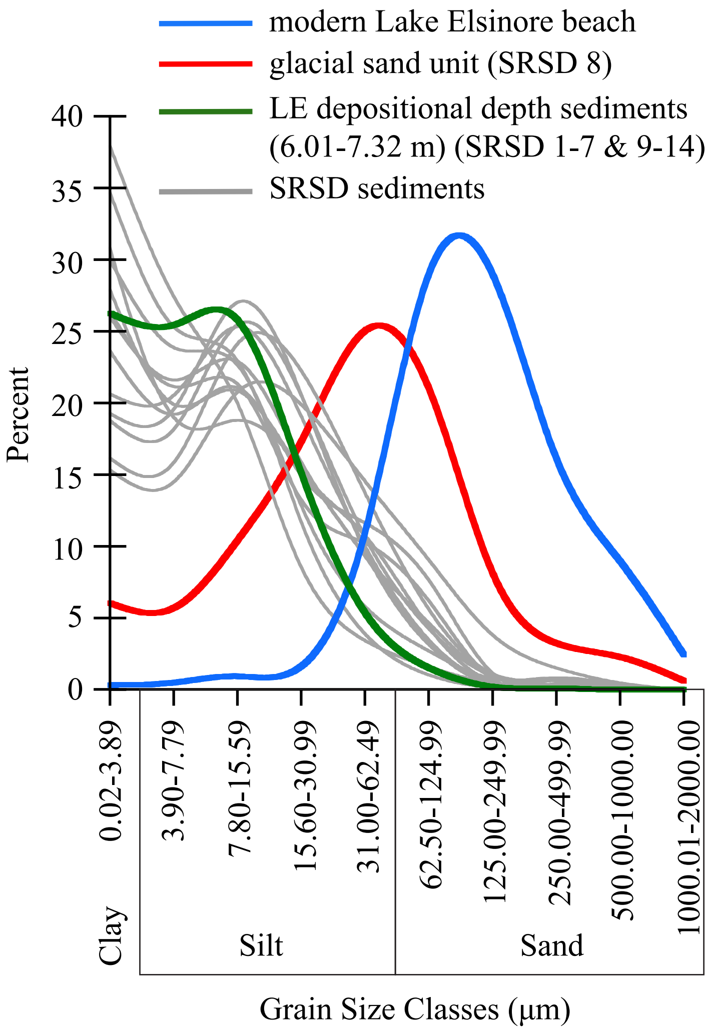
modern Lake Elsinore beach
glacial sand unit (SRSD 8)
LE depositional depth sediments (6.01-7.32 m) (SRSD 1-7 & 9-14)
SRSD sediments
Percent
40
35
30
25
20
15
10
5
0
0.02-3.89
3.90-7.79
7.80-15.59
15.60-30.99
31.00-62.49
62.50-124.99
125.00-249.99
250.00-499.99
500.00-1000.00
1000.01-2000.00
Clay
Silt
Sand
Grain Size Classes (µm)

Figure 6

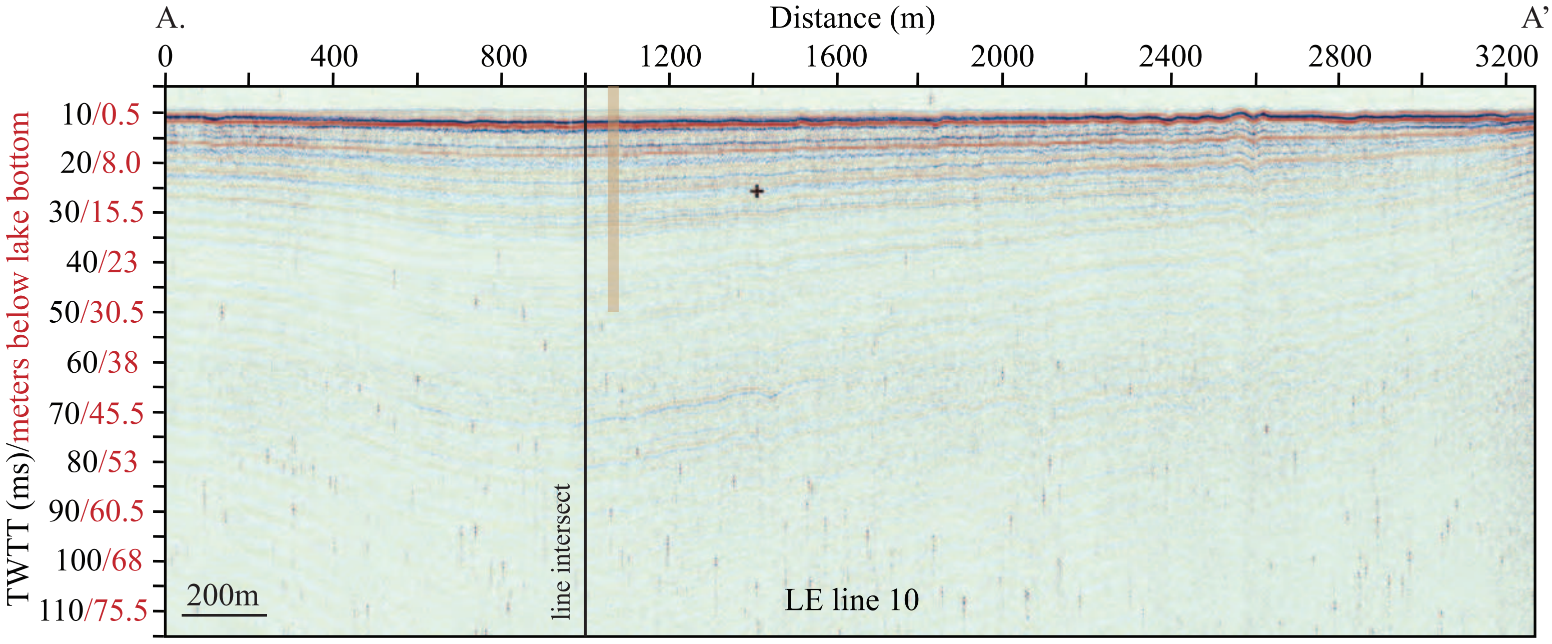
A.
Distance (m)
A'
0
400
800
1200
1600
2000
2400
2800
3200
TWTT (ms)/meters below lake bottom
10/0.5
20/8.0
30/15.5
40/23
50/30.5
60/38
70/45.5
80/53
90/60.5
100/68
110/75.5
200m
line intersect
LE line 10

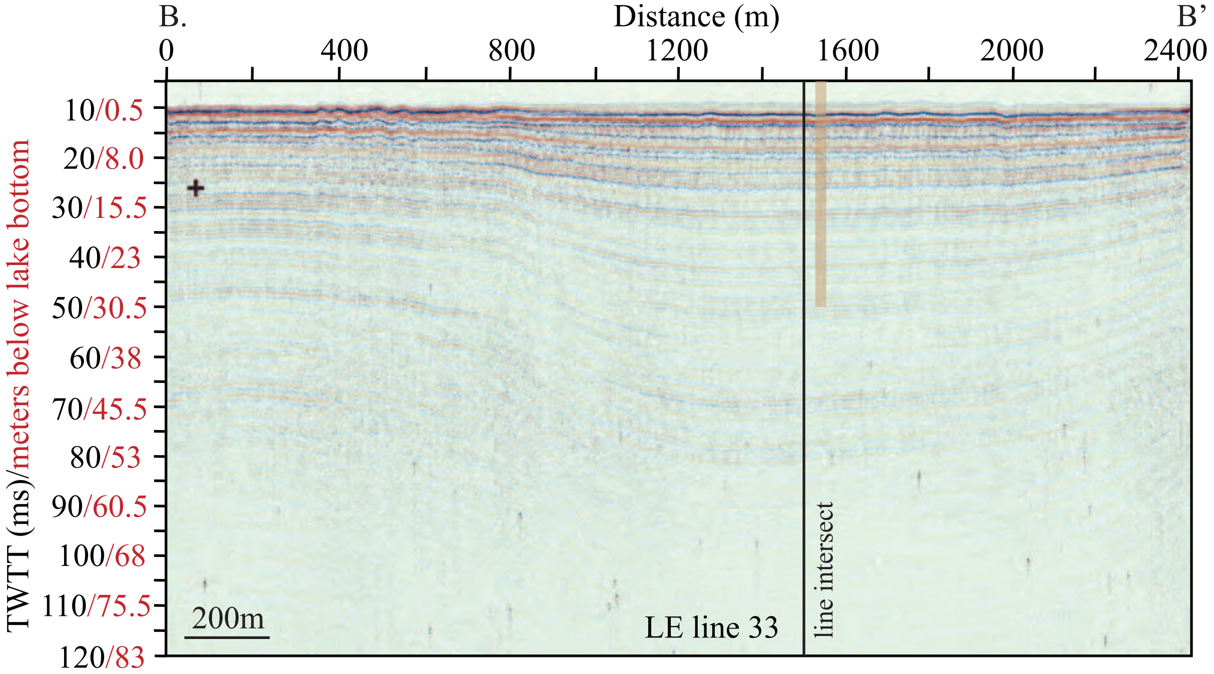
B.
Distance (m)
B'
0
400
800
1200
1600
2000
2400
TWTT (ms)/meters below lake bottom
10/0.5
20/8.0
30/15.5
40/23
50/30.5
60/38
70/45.5
80/53
90/60.5
100/68
110/75.5
120/83
200m
LE line 33
line intersect

Figure 7

Figure 8

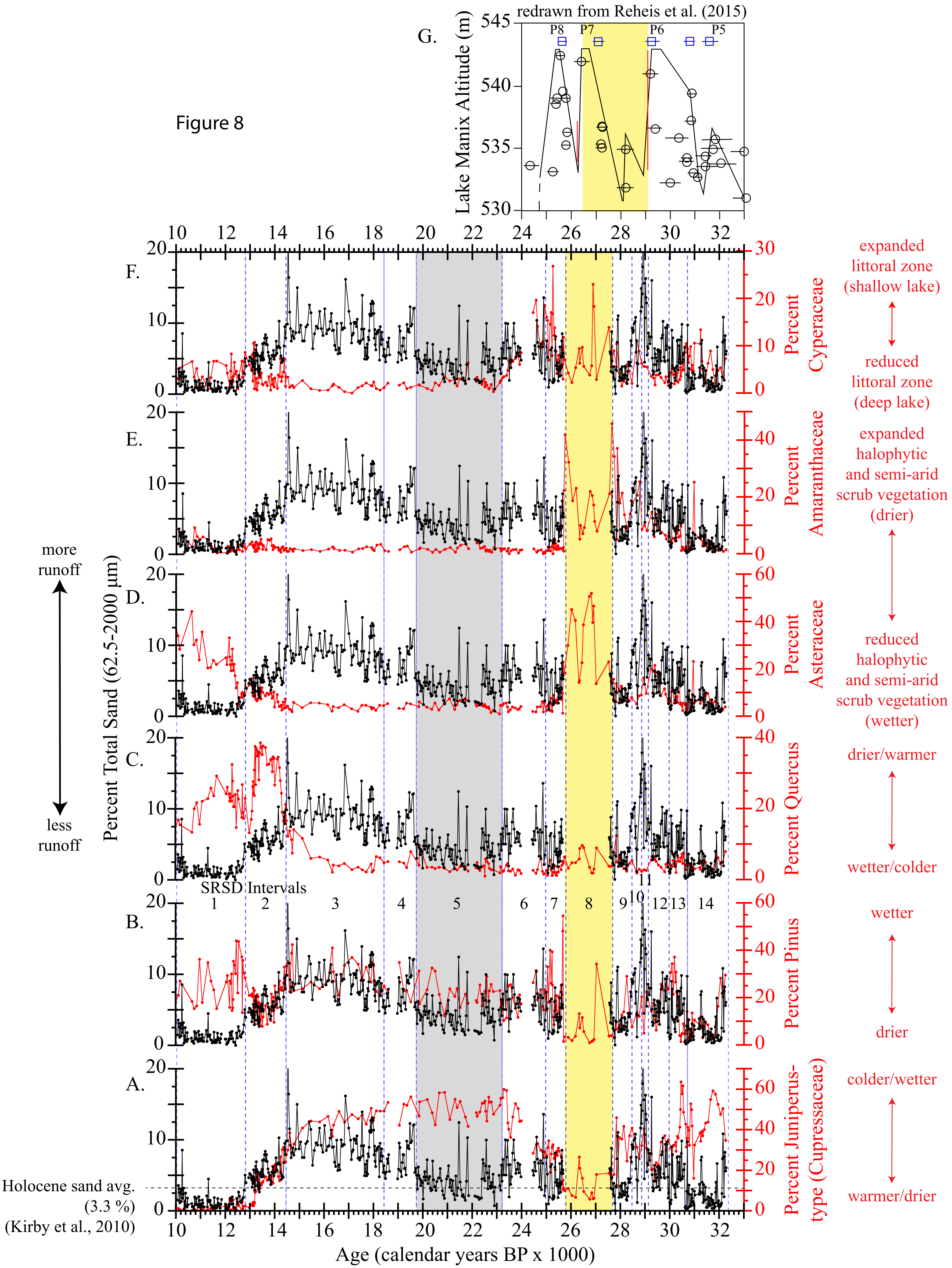
redrawn from Reheis et al. (2015)
G.
Lake Manix Altitude (m)
545
540
535
530
P8
P7
P6
P5
24
26
28
30
32
F.
E.
D.
C.
B.
A.
10
12
14
16
18
20
22
24
26
28
30
32
20
10
0
Percent Total Sand (62.5-2000 µm)
more runoff
less runoff
Percent Cyperaceae
30
20
10
0
expanded littoral zone (shallow lake)
reduced littoral zone (deep lake)
Percent Amaranthaceae
40
20
0
expanded halophytic and semi-arid scrub vegetation (drier)
Percent Asteraceae
60
40
20
0
reduced halophytic and semi-arid scrub vegetation (wetter)
Percent Quercus
40
20
0
drier/warmer
wetter/colder
SRSD Intervals
1
2
3
4
5
6
7
8
9
10
11
12
13
14
Percent Pinus
60
40
20
0
wetter
drier
Percent Juniperus-type (Cupressaceae)
60
40
20
0
colder/wetter
warmer/drier
Holocene sand avg. (3.3 %) (Kirby et al., 2010)
Age (calendar years BP x 1000)

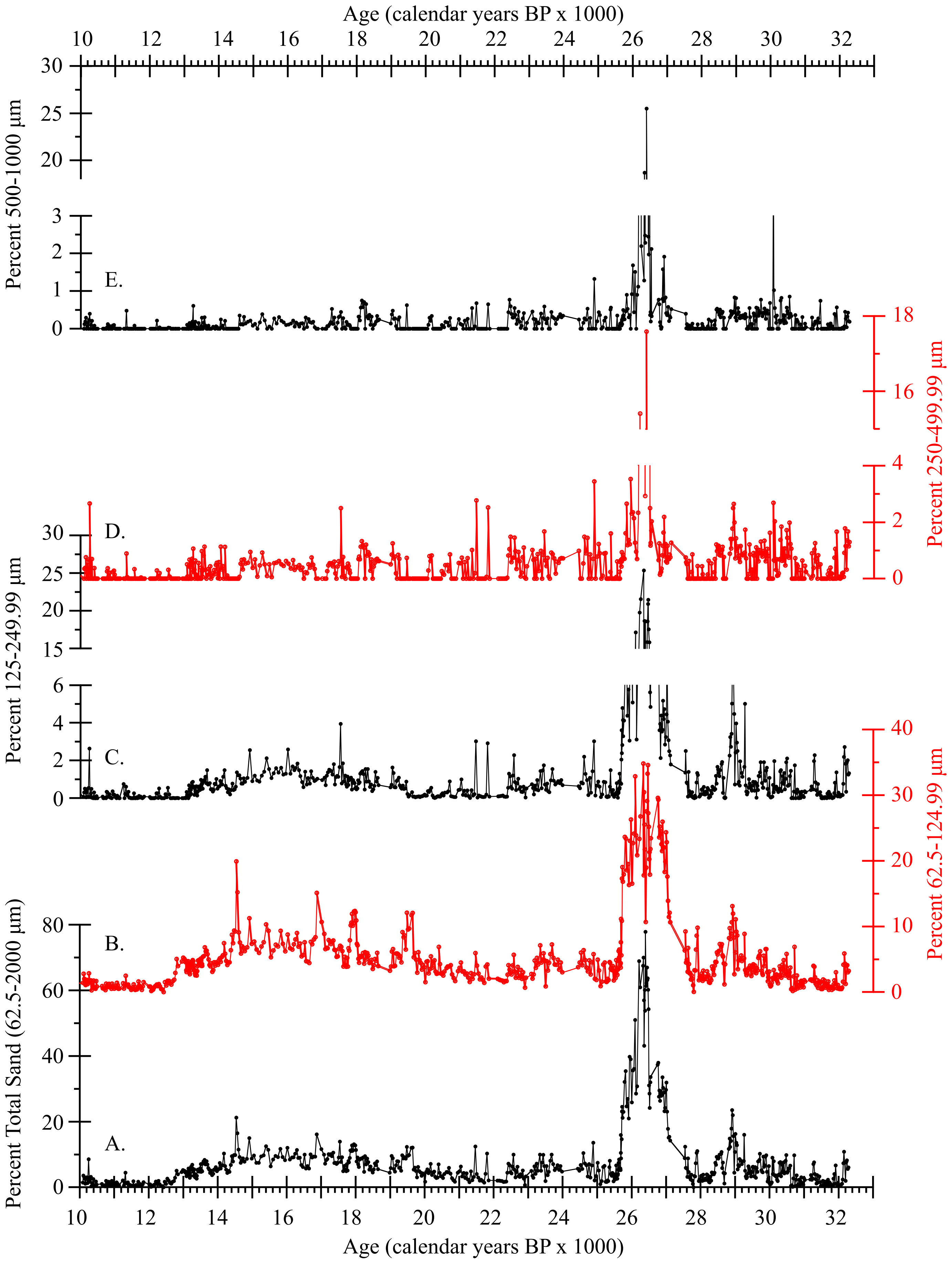
Age (calendar years BP x 1000)
10
12
14
16
18
20
22
24
26
28
30
32
Percent 500-1000 µm
30
25
20
3
2
1
0
E.
Percent 250-499.99 µm
18
16
4
2
0
D.
Percent 125-249.99 µm
30
25
20
15
6
4
2
0
C.
Percent 62.5-124.99 µm
40
30
20
10
0
B.
Percent Total Sand (62.5-2000 µm)
80
60
40
20
0
A.
Age (calendar years BP x 1000)

Figure S1

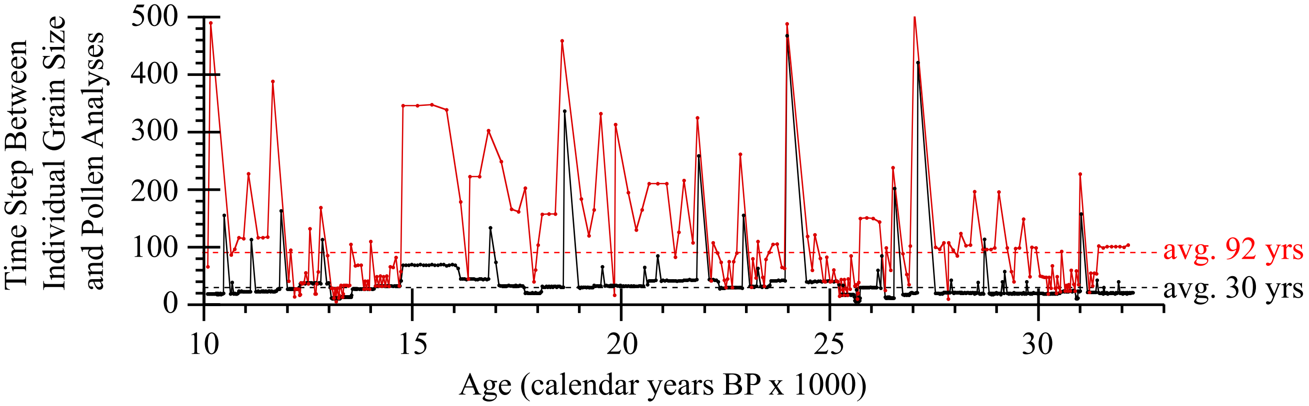
Time Step Between
Individual Grain Size
and Pollen Analyses
500
400
300
200
100
0
avg. 92 yrs
avg. 30 yrs
10
15
20
25
30
Age (calendar years BP x 1000)

Figure S2